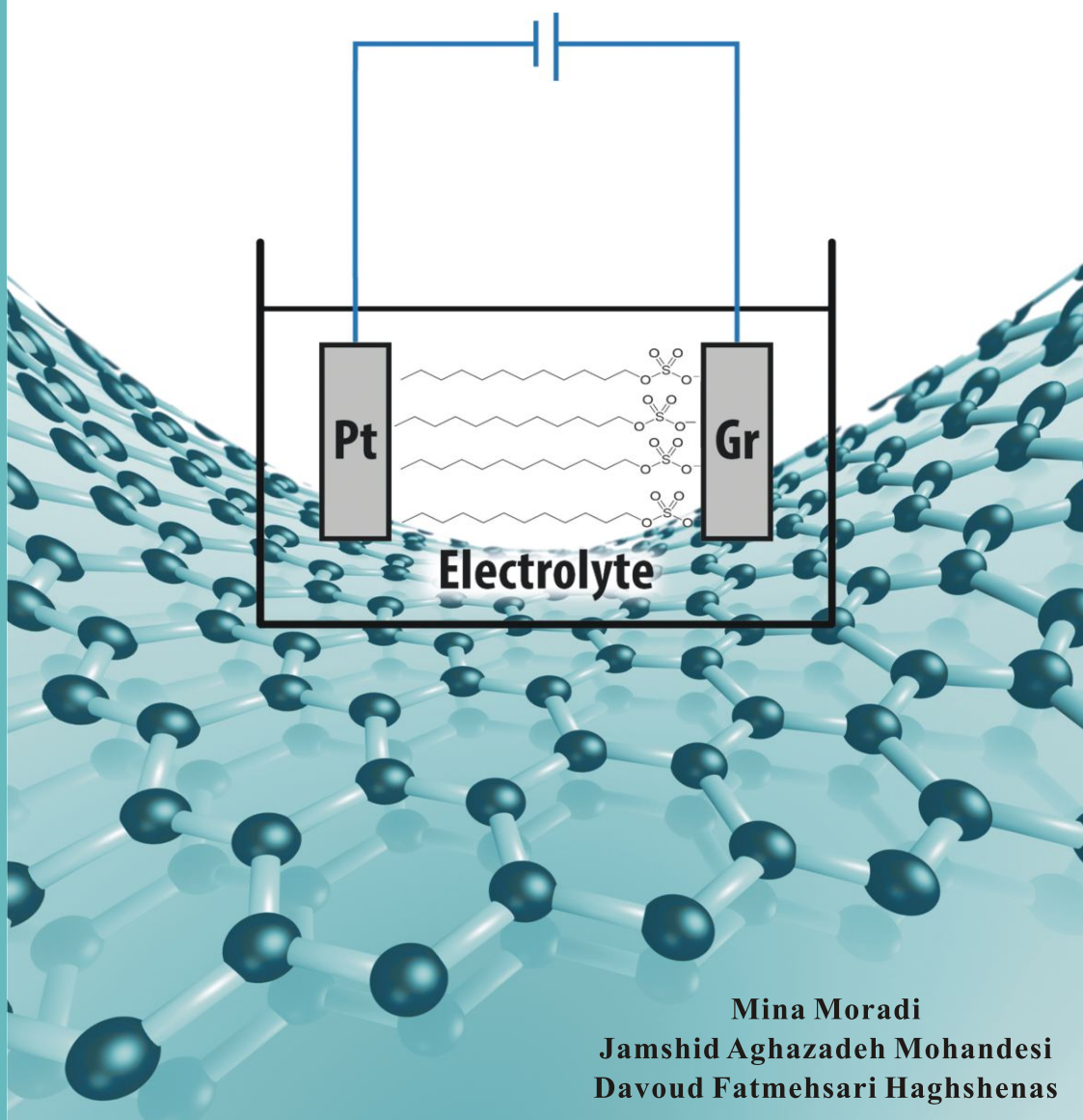


Electrochemical Fabrication and Mechanical Characterization of the Graphene/Poly Vinyl Alcohol Nanocomposites



Mina Moradi

Jamshid Aghazadeh Mohandesi

Davoud Fatmehsari Haghshenas

Electrochemical Fabrication and Mechanical Characterization of the Graphene/Poly Vinyl Alcohol Nanocomposites

Mina Moradi

Jamshid Aghazadeh Mohandesi

Davoud Fatmehsari Haghshenas

Science Publishing Group

548 Fashion Avenue
New York, NY 10018

www.sciencepublishinggroup.com

Published by Science Publishing Group 2015

Copyright © Mina Moradi 2015

Copyright © Jamshid Aghazadeh Mohandesi 2015

Copyright © Davoud Fatmehsari Haghshenas 2015

All rights reserved.

First Edition

ISBN: 978-1-940366-41-8

This work is licensed under the Creative Commons Attribution-NonCommercial 3.0 Unported License. To view a copy of this license, visit

<http://creativecommons.org/licenses/by-nc/3.0/>



or send a letter to:
Creative Commons
171 Second Street, Suite 300
San Francisco, California 94105
USA

To order additional copies of this book, please contact:

Science Publishing Group
book@sciencepublishinggroup.com
www.sciencepublishinggroup.com

Printed and bound in India

Contents

List of Symbols.....	V
Motivation	VII
Chapter 1 Introduction	1
1.1 Introduction	3
1.2 Graphene Properties	6
1.3 Fabrication Methods.....	8
1.3.1 Mechanical Exfoliation.....	8
1.3.2 Graphitization of Silicon Carbide.....	10
1.3.3 Chemical Vapor Deposition (CVD)	11
1.3.4 Annealing Solid Carbon Sources.....	13
1.3.5 Graphene Dispersion from Graphite.....	13
1.3.6 Chemical Preparation of Graphene.....	14
Chapter 2 Experimental Section	25
2.1 Experimental Section.....	27
2.1.1 Materials	27
2.1.2 Synthesize of the Graphene Sheets.....	27
2.1.3 Preparation of SWGSs/PVA Composites.....	28
2.1.4 Methods of Characterization	28
Chapter 3 Results and Discussion	31
3.1 Result and Discussion.....	33
3.2 Characterization of SWGSs.....	35
3.2.1 Chronoamperometry	35
3.2.2 Raman Spectroscopy	37

Contents

3.2.3 FT-IR Analysis	38
3.2.4 AFM Result	39
3.2.5 X-Ray Diffraction.....	40
3.2.6 Electron Microscopic Studies	41
3.3 Characterization of SWGSs/PVA Nanocomposite Films.....	43
3.3.1 XRD Patterns	43
3.3.2 Mechanical Properties	44
3.3.3 Thermal Studies.....	47
3.3.4 FE-SEM Studies	49
Conclusion.....	51
References	53
Appendix	65

List of Symbols

1,3-Dimethyl-2-Imidazolidinone	DMPU
3-Aminopropyltriethoxysilane	APTES
Atomic Force Microscopy	AFM
Calcium Nitrate	$\text{Ca}(\text{NO}_3)_2$
Calcium Dodecyl Sulfate	$\text{Ca}(\text{DS})_2$
Current–Time Transient	CTT
Carbon Nano Tube	CNT
Deionized water	DI water
Differential Scanning Calorimetry	DSC
Dodecyl Sulfate Anion	DS^-
Fourier Transform Infrared	FT-IR
Field Emission Electron Microscopy	FESEM
Gamma- Butyrolactone	GBL
Graphene Sheet	GS
Graphene Oxide	GO
High Resolution Transmission Electron Microscopy	HTREM
Highly Ordered Pyrolytic Graphite	HOPG
Non-Isothermal Crystallization Peak Temperature	T_p
N-Methyl-2-Pyrrolidone	NMP
N,N-Dimethyl Acetamide	DMA

Lists of Symbols

Nuclear Magnetic Resonance	NMR
Poly Acrylonitrile	PAN
Poly(vinyl alcohol)	PVA
Poly(methyl metacrylate)	PMMA
Polystyrene	PS
Self-Assembled Monolayer	SAM
Sodium Dodecyl Sulfate	SDS
Surfactant Wrapped Graphene Sheet	SWGS
Silicon wafer	Si wafer
Transmission Electron Microscopy	TEM
Thermo Gravimetric Analysis	TGA
X-Ray Diffraction	XRD

Motivation

The challenges in nanotechnology and especially in carbon nanostructures can be considered in two aspects, the preparation/fabrication of the nanostructures and their properties regarding the specific applications. In order to explore and exploit the rich physics/chemistry of the graphene, new methods are required to tailor their properties. This book which is based on a master thesis is a contribution to the both above mentioned aspects through the following goals:

- Exploring a novel route for the synthesis of a stable suspension containing graphene sheets in aqueous solution.
- Characterization of the produced graphene sheets.
- Developing the Graphene/Poly(vinyl alcohol) nanocomposites.
- Evaluation of the mechanical properties of the nanocomposites.

Chapter 1

Introduction

1.1 Introduction

Carbon in the form of coal had been the driving force of the industrial revolution. Nowadays, the carbon nanostructures play a significant role in another technological/scientific revolution: nanotechnology. The research in the realm of carbon nanotechnology has been significantly contributed to the routes which the science has taken at the nanoscale. The carbon nanostructures include fullerenes, carbon nanotubes and recently prepared single layers of graphite; graphene [1]. Although, all of the above mentioned carbon advanced materials are composed of sp^2 carbon, the physical/chemical properties of them vary due to by versatile atomic structures. Carbon has four valence electrons with similar energies which can easily hybridize. In carbon atom, these valence electrons give rise to $2s$, $2p_x$, $2p_y$, and $2p_z$ orbitals while, the two inner shell electrons which belong to a spherically symmetric $1s$ orbital; are tightly bound and the energy level of them is far from the Fermi level of carbon. Thus, only the electrons corresponding to the $2s$ and $2p$ orbitals contribute to the solid-state properties of graphite. This unique capability for hybridization makes the carbon to form 0D, 1D, 2D, and 3D structures (Fig. 1.1).

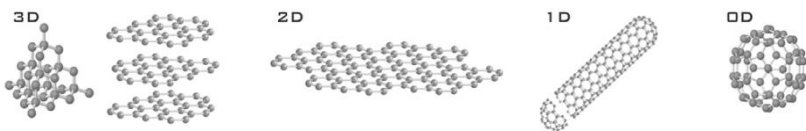


Fig. 1.1 Different structures of carbon allotropes [2].

During the 1960s and 1970s, carbon fibers became an important industrial material [3] and today, they employ in variety fields from sports equipment to vehicle parts, anywhere where the low weight together with high strength is required. Fibrous carbon materials are as part of everyday life in the form of

carbon fiber reinforced composites [3]. Carbon nanotubes and graphene promise even greater benefits if their extraordinary properties can be harnessed. In the last few years graphene, which consists of a single layer of carbon atoms arranged in a honeycomb lattice, has become one of the most interesting and controversial topics in physics and material science [4, 5]. The word of graphene is derived from the word graphite and the suffix-ene that is used for polycyclic aromatic hydrocarbons such as naphthalene, anthracene, coronene and benzene [6]. Thus, the term graphene refers to one strictly two-dimensional monolayer of graphite in the (0001)-plane.

The hexagonal structure is also a well-known for carbon nanotubes and, somehow, for fullerenes [7]; i.e. this structure has been theoretically studied for a long time as a building block of graphite and carbon nanotubes (Fig. 1.2) [7].

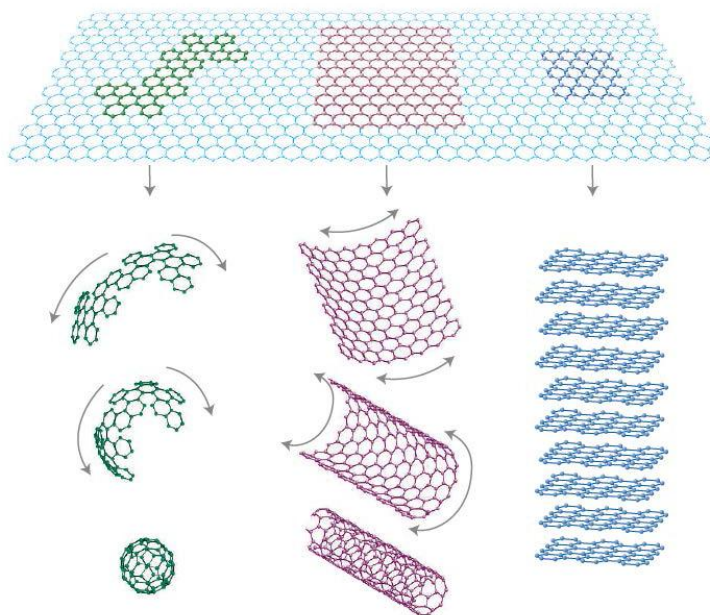


Fig. 1.2 Graphene, a single sheet of graphite, can be considered as a building block of all these carbon structures [8].

Since in graphite the distance between the graphite planes is high in compared to that of carbon atoms within the same plane (3.37 Å versus 1.42 Å), graphene serves as a model particularly for the description of such 3D material [9, 10]. In 1937 Landau had theoretically stated that 2D crystals were thermodynamically unstable [11], and consequently, the 2D crystal system such as graphene was only theoretically discussed. Still, many experimentalists have acquired graphene as an unwanted byproduct during experimental runs in the laboratory. In fact, the structural study on the other forms of carbon nanostructures, fullerenes and carbon nanotubes, helped to the rapid development of the graphene identification and characterization. Graphene as a thin film over the metallic substrates was produced and studied at the 1970s when Blakely and colleagues worked on the single layer graphite growth over the various transition-metal substrates [12, 13, 14]. Van Bommel et al. developed graphene/thin graphite films by silicon evaporation of SiC in 1974 [15] even former, the separation of graphene layers via the intercalation/exfoliation of graphite and so called graphene oxide were investigated [16, 17]. However, the first documented graphene synthesis as a carbon monolayer was recorded in 1977 by Oshima et al. It is worthy of note that acquiring a clean crystal surface was difficult in the case of materials which tend to dissolve carbon atoms; as a result, it was usually more convenient to study the carbon covered clean surfaces [17, 18, 19]. Since the most research on graphene was practically conducted over the metal substrates, the properties of graphene were not completely preserved in such systems. At 1986, Till Boehm et al. proposed the term “graphene” for the description of a single atomic sheet of graphite [6]. Finally, Novoselov et al. at 2004 could produce free-standing graphene flakes from the graphite crystals by mechanical exfoliation [20]. Following these findings, Novoselov et al. [20, 21], Zhang et al. [23] and Berger et al. [23] have quantified very unique properties of graphene. However, despite

many fundamental researches on the graphene, the production of high quality graphene for applied purposes has been still a challenging issue.

1.2 Graphene Properties

At a glance, Graphene is immediately considered as the successor of current silicon-based technology due to the 2D honeycomb carbon structure, which makes it ideal as a computing element. Therefore, graphene sheets can be potentially used in computer technology. Moreover, pure graphene exhibits exceptional mechanical, physical and chemical properties such as Young's modulus (~ 1000) [24], thermal conductivity ($\sim 5000 \text{ Wm}^{-1}\text{K}^{-1}$) [25], mobility of charge carriers ($\sim 200\,000 \text{ cm}^2\text{V}^{-1}\text{s}^{-1}$) [26], and specific surface area ($\sim 2630 \text{ m}^2\text{g}^{-1}$) [27] while, graphene derivatives like graphene oxide or other types of functionalized graphene display remarkable catalytic, mechanical, sensing and electronic properties.

One of the most important factors that enabled the discovery of single layer graphite among these crystallites is that even graphene, not to mention bilayer graphene, can be seen with a conventional optical microscope on top of a wafer with carefully chosen SiO_2 thickness [20, 28]. This effect arises because graphene has certain opacity and it also adds to the optical path of the light traversing the SiO_2 capping layer [28]. Together, these effects are enough to give graphene a well discernible contrast in an optical microscope. This technique simplifies the process of finding single graphene sheets but obviously limits this fabrication scheme to devices for research purposes.

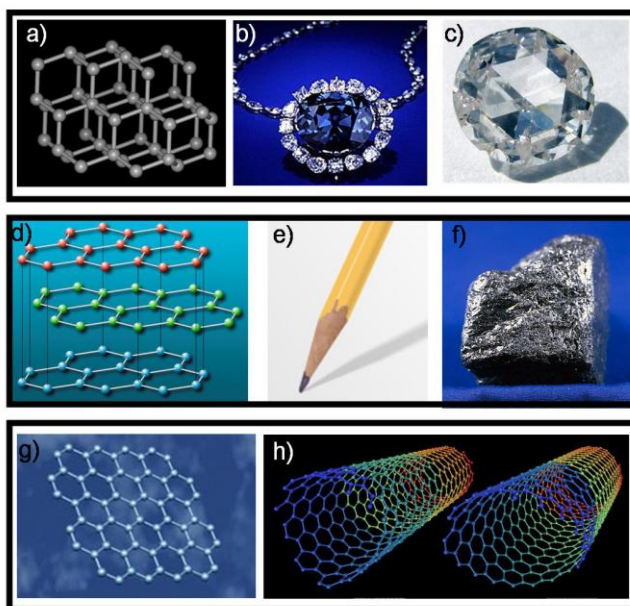


Fig. 1.3 (a) Diamond lattice. Picture taken from <http://mrsec.wisc.edu> (b) Hope Diamond. Image from Smithsonian. (c) Lab grown diamond. Image from Apollo diamond, Inc. (d) Graphite lattice. Image from. <http://www.scifun.ed.ac.uk/> (e) Pencil. Image from www.xara.com. (f) Graphite. Image from U.S. Geological Survey. (g) single layer of graphene. Image from <http://ewels.info.com>. (h) Single walled carbon nanotubes. Image created by Michael Ströck from Wikipedia.

Fig. 1.3 shows the 2D sp^2 hybridized structure of Graphene and Graphite. Actually, Graphite is the stacks of graphene sheets with 0.3 nm distance between the layers. These layers held together by weak Van Der Waals forces (Fig. 1.3 d) [9]. Thus, they can slide relatively easily across each another. It has been known that the presence of water molecules reduce the frictional force considerably [29, 30]. Another frictional effect which is believed to be important is the registry of the lattice between the layers. A mismatch in this registry gives graphite the property of superlubricity where the frictional force reduces significantly [31]. Mechanical experiments based on few layer graphene may help to elucidate some of these mechanisms clearly [32].

A single 2D sheet of graphene has hexagonal structure and each atom forms three bonds with each of its nearest neighbors (Fig. 1.3g). These are known as the bonds oriented towards the neighboring atoms. These covalent carbon-carbon bonds, the strongest bond in nature, lock these atoms in place giving them remarkable mechanical properties [33, 34]. In other words, the covalent C-C bonds in graphene are nearly similar to those present in diamond structure. Interestingly, a suspended single layer of graphene is one of the stiffest known materials with a Young's modulus of ~ 1 TPa. The fourth valence electron that does not participate in covalent bonding is located in the $2p_z$ state perpendicular to the sheet of graphite (a conducting π band).

The mechanical properties of graphene are still unexplored and it is the time to revise the old assumptions about bulk graphite for determination of the elastic constants by scaling down it to the atomic thicknesses. In this regard, production single atomic layers or few atomic layers of graphene can be useful for overcoming some of the uncertainties involved in working with large single crystals.

1.3 Fabrication Methods

1.3.1 Mechanical Exfoliation

The most widely used method is which the single layer graphene flakes are mechanically separated from the bulk graphite. Carbon layers in bulk graphite are held together by weak Van Der Waals energy of the order of 2 eV/nm^2 and a force about $300 \text{ nN}/\mu\text{m}^2$ is adequate for removing the monolayer of graphene [35]. Such small force can be easily produced by an adhesive tape. In 2004 Novoselov et al. used common "scotch" tape to peel off layers of graphite from HOPG [1].

This so called micromechanical cleaving technique consists of repeated peeling off the graphite crystallites stuck to the scotch tape, during which ever thinner crystals are produced on the tape surface. In fact, this method of graphene fabrication is exfoliation, the technique that has been employed for centuries; i.e. writing with a graphite pencil over a paper. During writing with a pencil, many graphene sheets spread over the paper but in an uncontrollable way. In this way, the graphite crystals separate very easily because of the weak Van Der Waals forces. After peeling, the tape is pressed against the surface of a silicon wafer having either a 90 or 300 nm of SiO₂ capping layer. While the tape is removed from the surface of the wafer the crystallites sticking to the SiO₂ surface cleave one last time and the result is an assortment of graphite crystals with varying thicknesses on the SiO₂ (Figure 1.4 b). To distinguish between layers of graphene, the thickness of SiO₂ is important because at the thickness of 90 nm or 280 nm, graphene contrast on SiO₂ is maximized by about 12% at 550 nm where the sensitivity of human eye is optimal [28].

To partially remove contamination from adhesive tape, heat treatment under Ar/H₂ atmosphere at 200 °C [36] or in situ Joule heating by the application of current of the order of micro amperes can be employed [37]. The size of graphene flakes obtained by this method is limited which is the main obstacle towards large scale graphene production. However, this method is the benchmark for the comparison of the electronic characteristics of the graphene obtained by other techniques.

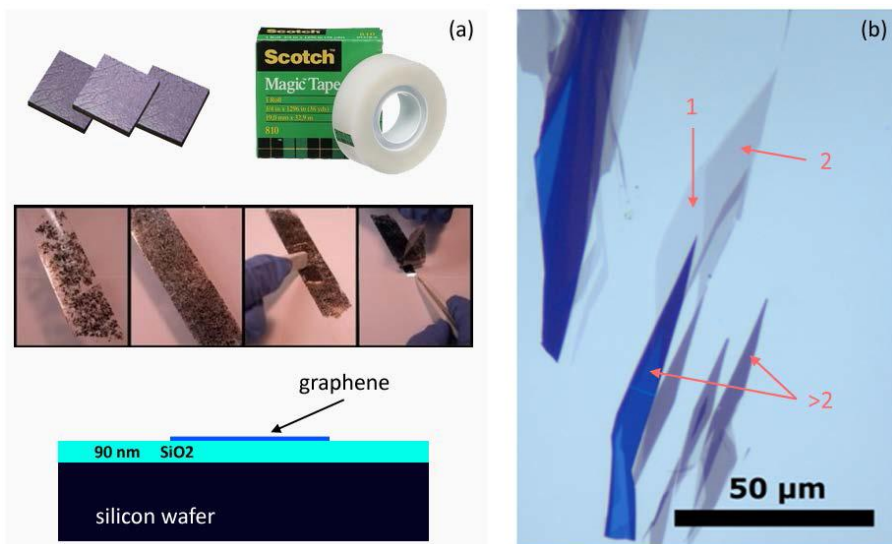


Fig. 1.4 (a) Process of preparing graphene (b) Optical microscopy image of single layer graphene on 90 nm thick SiO₂ Single, bi- and multi layered graphite is highlighted by the red arrows.

There are recent attempts to improve the quality and yield of exfoliation techniques. These include stamping methods which use silicon pillars to transfer graphene flakes and electrostatic voltage assisted exfoliation which uses electrostatic forces to controllably separate graphene from bulk crystals [38].

1.3.2 Graphitization of Silicon Carbide

Another route for the production of graphene sheets is the graphitization of silicon carbide. In this method the SiC wafer, a highly resistive material, is heated up to 1200-1400 °C. This heat treatment results in the removal of surface silicon and a carbon rich phase is left which consists of graphene layers [39]. This process is ideally suited for future electronics applications since graphene covers the entire surface of the SiC wafer and the substrate. However, the graphene prepared via this method has higher crystal defects than the cleaved graphene [23].

It should be noted that direct growth of graphene currently has the highest potential for mass production purpose. Typically, this technique is accomplished by heating a SiC wafer resulting in the partial graphitization of the upper layers [40, 23]. However, the control over the number of layers together with the grain size is difficult [23]. Furthermore, lithography is required for the isolation of the single sheets to pattern the electrostatic gates on top of the graphene surface. Another disadvantage of the high temperature vacuum annealing of SiC is the highly corrugated surface covered by small graphene regions with various thickness [41]. In order to overcome this problem, the use of carbon terminated SiC has been proposed instead of previously used Si terminated SiC [42]. However, higher graphene coverage via this method has been achieved by graphitization near atmospheric pressure (Ar atmosphere at ambient temperature) resulting in a smooth surface with graphene coverage (50 μm) [43]. The problem with this technique is the initial costs of the SiC wafer and high operational temperature (1400-1600 $^{\circ}\text{C}$).

1.3.3 Chemical Vapor Deposition (CVD)

Carbon nanotubes and diamond are successfully grown via CVD methods. Similar to the CNTs, CVD methods are one of the most important methods for graphene preparation which enable the growth of graphene samples of macroscopic size [44, 45].

This technique is based on the usage of precursors in the vapor phase which adsorb and react over the substrate surface at elevated temperatures under low pressure or atmospheric pressure; this results in the deposition of thin film through the chemical reactions. In case of graphene, the precursors are typically carbon containing gas/vapors such as methane and alcohols that react over the transition metal surface under the ambient environment in which the deposition

of amorphous carbon is avoided. The transition metals serve as the efficient catalysts in transformation of hydrocarbons into the graphitic materials [46], for instance, in early 1960's graphite layers were obtained over nickel surface from hydrocarbon gases (vapors) or evaporated carbon [47]. The solubility of carbon in transition metal during CVD process has an important role in growth mechanism and the number of graphene layers [47]. Recent research on graphene growth over the copper substrate (Fig. 1.5) indicates that CVD can result in the growth of monolayer graphene with high coverage; this is due to the negligible solubility of carbon in copper even at 1000 °C [50].

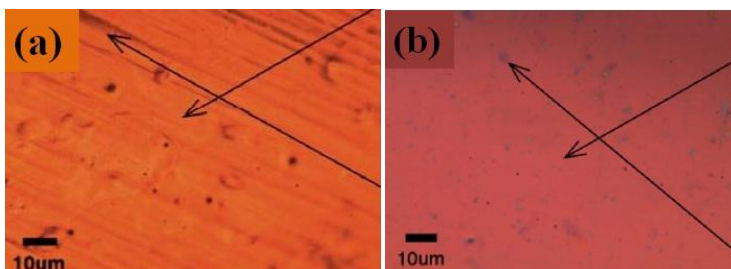


Fig. 1.5 CVD grown graphene on copper. Optical images of (a) as-grown graphene and (b) transferred to 300 nm SiO₂. Black arrows in (a) show corrugations on copper surface that result in multilayer graphene highlighted by black arrows close to purple regions in (b) [48].

Since the graphene growth on copper is surface limited, the smoothness of copper surface plays very significant role in obtaining monolayer coverage across entire surface of the substrate [49]. Using this process, the size of graphene is only limited by the size of the metal substrate. Additionally, it should be mentioned that graphene obtained by CVD is inferior in compared to graphene obtained by mechanical exfoliation in terms of above mentioned parameters. One reason for such inferiors is that the graphene obtained via CVD is a continuous sheet which is inherently polycrystalline because the different orientated domains of graphene merge to form a graphene sheet. Also, due to the presence of grain boundaries,

the electrical properties of the film are poor [50]. Many efforts have been devoted to obtain the single crystal isolated graphene domains with improved electrical properties [51]. Another major problem with CVD is that graphene is located over a metal surface and for the electronic devices, it is necessary to have graphene on an insulating substrate such as SiO₂. During the transfer of graphene from a conducting substrate to an insulating one, unavoidable structural damages occur for graphene, which can degrade its electronic/ electrical properties [52].

1.3.4 Annealing Solid Carbon Sources

In this method, the carbon precursor is solid such as PMMA [53], amorphous carbon [54] on copper surface, PAN, PS, PMMA [55], C60 [56] on nickel surface which is usually evaporated or spin coated over the metal surface. Another implementation method of this process is the deposition of carbon source on SiO₂/Si and then metal thin film is evaporated/annealed at elevated temperatures. The advantage of such method is that there is no need to transfer graphene to an insulating substrate. This has been also demonstrated in the case of C60 [56] and SAM [57] on nickel thin film evaporated on SiO₂/Si.

One advantage of this method is that in situ doped graphene can be obtained by using solid carbon precursors that also contains desired dopant element [57]. The limitations of the method are similar to those corresponding to CVD. It is worthy of note that this method is relatively new and the physicochemical aspects of graphene formation are still the topic of active research.

1.3.5 Graphene Dispersion from Graphite

In this method graphite flakes are sonicated in a solution and then dispersed onto a wafer. AFM analysis is used to locate individual sheets [58]. This tech-

nique is very time consuming compared to the optical detection. Long sonication time is required to break the graphite and obtain small flakes [59]. One difficulty in dispersing graphene in the solution is the careful separation of the layers without destroying. The intercalation of graphite and dispersing in a solvent is one method to prevent such destruction. This technique is effective for graphene oxide. However, the aggregation of graphene sheets is another problematic issue.

1.3.6 Chemical Preparation of Graphene

Among the above mentioned methods for the synthesis of graphene sheets, the chemical production routes are the most promising in terms of controlling the process parameters and quality/quantity of the layers (transparency, sheet size and related features such as defect/impurity levels and reinforcing role in polymer matrix). In fact, while, micromechanical cleavage is very successful in producing samples for fundamental studies, the extremely low yield and lack of control in placement of the sheets, limits its application. Other methods based on the use of SiC as a substrate and as a precursor have excellent potential in the pursuit of the best quality synthetic graphene but they are too expensive. For large scale production of GSs, graphite is used as starting material and delaminating is carried out by various means such as chemical functionalization, oxidation or intercalation. The idea behind this technique is to intercalate different reactants among the bulk graphite which results in the separation of graphite layers. In some of these methods, chemical oxidation of graphite precursor occurs and graphene oxide forms; the subsequent exfoliation and reduction lead to reduced graphene oxide nanosheets [60].

The challenge to this approach is that the original sp^2 network of graphite is not restored even after the treatment with reducing agents. To overcome this problem, non-covalent functionalization of conjugated carbon network can be a

proper alternative. The advantage of this scheme is that the external functional groups attach to carbon network through π - π stacking rather covalent bond formation. These improvements are the basis of other methods which employ direct intercalation and exfoliation of graphite (electrochemical methods) and produce a suspension of graphene sheets.

(a) Synthesis of Graphene from Graphene Oxide

In the first report on the production of GO [61], natural graphite (Ceylon) was treated by an oxidative mixture of potassium chlorate and fuming nitric acid for 3–4 days at 60 °C until no change was observed. After many years, Hummers and Offeman developed a method in which the oxidation of graphite was accomplished by treating a mixture of concentrated sulfuric acid, sodium nitrate and potassium permanganate (Fig. 1.6). This process required less than 2 h for completion at lower temperatures (below 45 °C) [16].

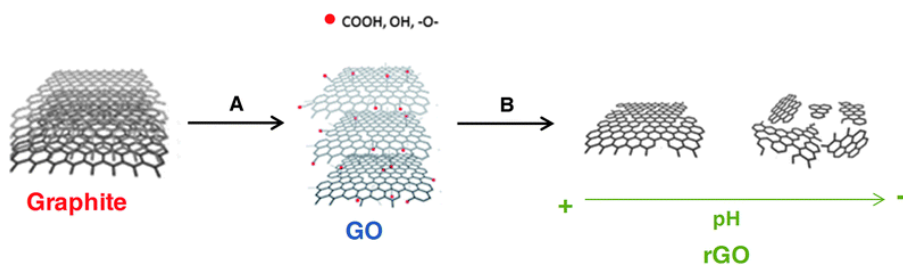


Fig. 1.6 Hummer's method to produce graphene sheet [16].

Based on the results obtained with a variety of modern analysis techniques such as NMR, XPS, TEM and Raman, the most recent model of GO structure is schematically depicted in Figure 1.7, where hydroxyl and epoxide groups are randomly grafted to the carbon mesh and alter the sp^2 -bonded carbon network of pure graphene sheets.

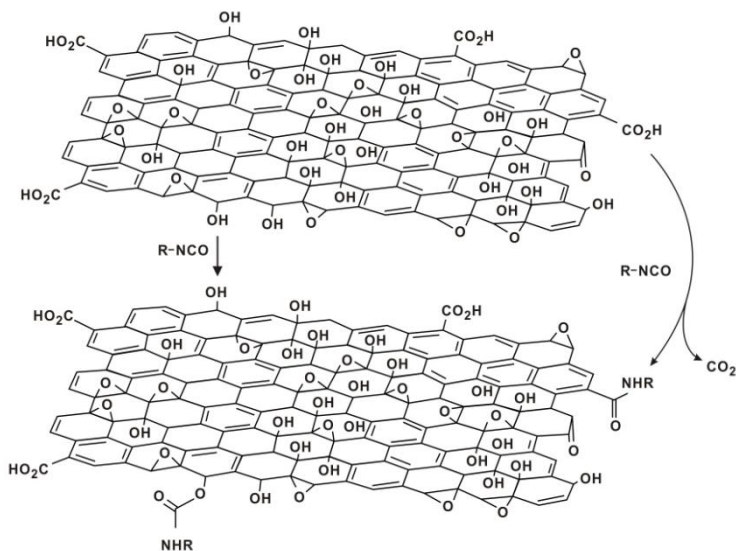


Fig. 1.7 Structure of graphene oxide [62].

Regarding the desired properties depending on the application, graphene/graphene oxide is processed by several steps. On the other hand, the fabrication of graphene and/or graphene oxide composites coupled with a polymer or other layered material such as clay is another important goal of research. Some of these composite materials do not require any reduction process and the graphene oxide is utilized; for instance, the GO paper introduced by Ruoff and coworkers [63] is a well-known example of such composite films.

Nowadays the most efficient procedure for the reduction of GO seems to be the H plasma reduction method proposed by Kern et al [64]. Another efficient method is the thermal treatments or heat treatments in the vacuum or controlled atmosphere conditions [65]. Moreover, another alternative approach is the reduction of graphene oxide using electrical energy [66].

(b) Liquid-Phase Exfoliation of Graphite

Chemical preparation of graphene without oxidation is the way for the production of graphene sheets. A very influential method for the exfoliation of graphite is the use of organic solvents such as NMP, DMA, GBL and DMPU [67] (see appendix A). Such solvents have interaction energy with graphene equal to graphene–graphene interaction energy which results in a minimal energy to overcome the Van Der Waals forces between the graphene sheets.

In the liquid-phase exfoliation method for producing graphene which it was employed by Lotya et al. [68], there is no need to oxidation or high temperatures which avoids using expensive solvents. In this technique, graphite is dispersed in surfactant aqueous solutions similar to surfactant aided carbon nanotube dispersion. The dispersed graphitic/graphene flakes are stabilized against re-aggregation by Coulomb Repulsion between the adsorbed surfactant molecules.

It is worthy of note that the aqueous systems has some specific advantages. Generally, the majority of the few-layer flakes have a lateral dimension of $\sim 1 \mu\text{m}$.

Considerable efforts have been dedicated to the chemical exfoliation of graphite without the oxidation of the graphene flakes which prevents severe damage of the graphene structure. A scalable and facile technique for non-covalent functionalization of graphene was proposed by An et al. [69] based on the π -stacking bond of this molecule with the graphitic surfaces. In this technique, the single-, few-, and multilayered graphene flakes are exfoliated in a stable aqueous with the help of 1-pyrenecarboxylic acid. The -COOH groups present in the 1-pyrenecarboxylic acid structure desire the polar medium

and in this way, they keep the graphene flakes as a stable suspension in water [74].

(c) Electrochemical Method

The electrochemical intercalation and exfoliation of graphite has recently grabbed many attentions because of various advantages compared to other methods.

The term intercalation refers to the accommodation of guest molecules or ions (called intercalants) into a host lattice possessing, in most of the cases, a layered structure. The insertion of guest species into the host matrix is exploited by the well-known ‘intercalation chemistry’. According to the type of interaction between intercalant and host material, intercalation may occur through (a) electrostatic interaction, due to ion exchange of interlayer metal cations with organic/inorganic cations (usually in clay minerals), (b) covalent binding via chemical grafting reactions within the interlayer space (e.g. of graphite) or (c) weaker interactions like Van Der Waals forces, hydrogen bonding, ion dipole and coordination, electron transfer, through absorption of neutral molecules by interaction with external or internal surfaces [70]. Graphite occupies a dominant space among the host matrices due to the high degree of structural ordering leading to well defined structures. The first synthesis of intercalated graphite was reported by Schaff \ddot{u} lt in 1841. However detailed studies of graphite intercalation compounds (GIC) began in the 1930s, with Hoffman; they introduced X-ray diffraction for the study of hybrid compounds structures [71]. During recent years GIC have attracted the scientists’ interest due to their fascinating applications in high electrical conductors [72], lithium-ion battery anodes [73], hydrogen storage materials, electrochemical storage media [74], separation processes and gas sensors. GICs are being used

extensively as the starting materials for obtaining colloidal dispersions of single-layer graphene sheets [75]. Ideally the use of a GIC allows the production of high quality graphene.

Liu et al. [66] showed the ionic-liquid-functionalized graphite sheets with the assistance of an ionic liquid and water are accessible through a mild one-step electrochemical process (Fig. 1.8). During this process the ionic-liquid-treated graphite sheets can be exfoliated into functionalized graphene nanosheets; this means that not only an individual and homogeneous distribution in polar aprotic solvents is achieved, but also there is no need to further deoxidization.

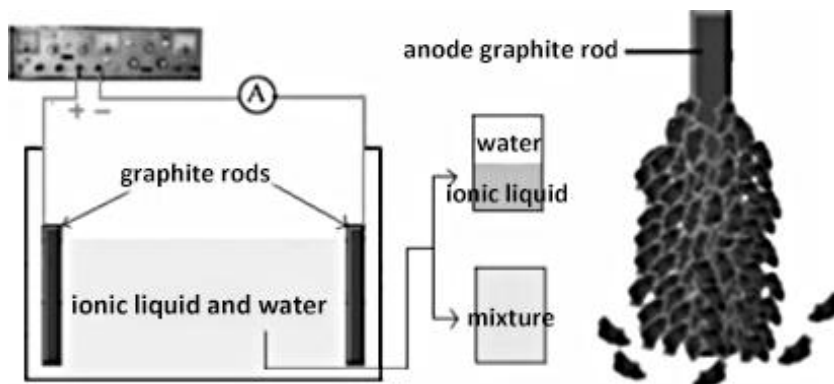


Fig. 1.8 Experimental set-up diagram (left) and the exfoliation of the graphite anode (right) [66].

One year later, highly efficient and large-scale synthesis of graphene from graphite was conducted by Wang et al. [76] via electrolytic exfoliation using poly (sodium-4-styrenesulfonate) (Fig. 1.9). Their results confirmed the existence of monolayer graphene sheets and presence of few graphene sheets in the stacks.

In other study, high-yield synthesis of few-layer graphene flakes through electrochemical expansion of graphite in propylene carbonate electrolyte has been carried out by Wang et al. [77]. A negative graphite electrode was

electrochemically charged and expanded in an electrolyte of Li salts and organic solvents under high current density; this led to efficient exfoliation of graphite into few-layer graphene sheets with the aid of sonication (Fig. 1.10).

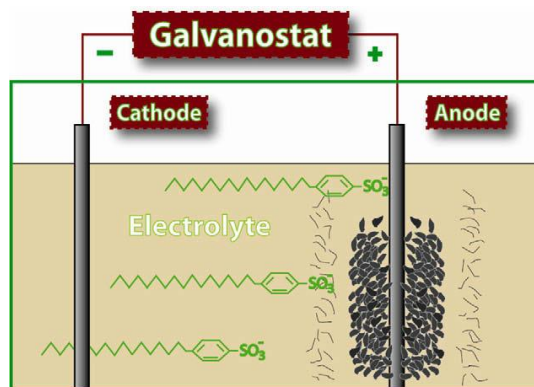


Fig. 1.9 Diagram of the apparatus for graphene synthesis via electrolytic exfoliation [77].

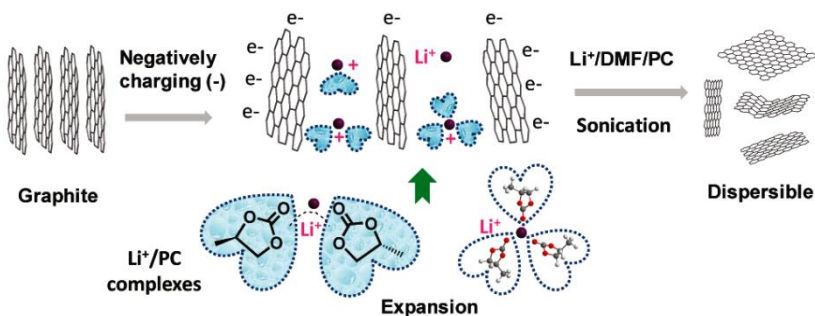


Fig. 1.10 Exfoliation of graphite into few layer graphene via Intercalation of Li^+ Complexes [77].

The one-step process for the production of high quality thin graphene films from a rapid electrochemical exfoliation has been reported by Su et al. [78] (Fig. 1.11). Their findings show that the lateral size of the exfoliated graphene sheets is in the range of several up to 30 μm , which significantly reduces the number of intersheet junctions for making percolative transparent conductive films.

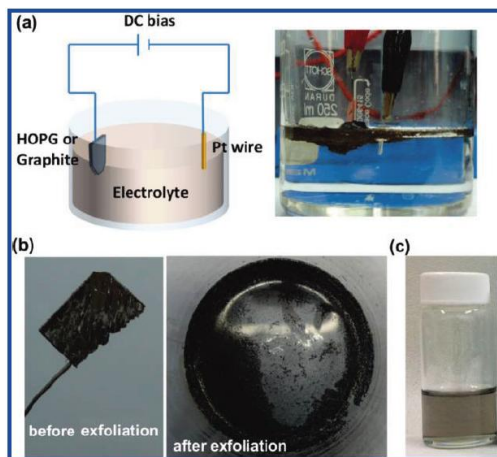


Fig. 1.11 (a) Schematic illustration and photo for electrochemical exfoliation of graphite. (b) Photos of the graphite flakes before and after electrochemical exfoliation. (c) Photo of the dispersed graphene sheets in a DMF solution [78].

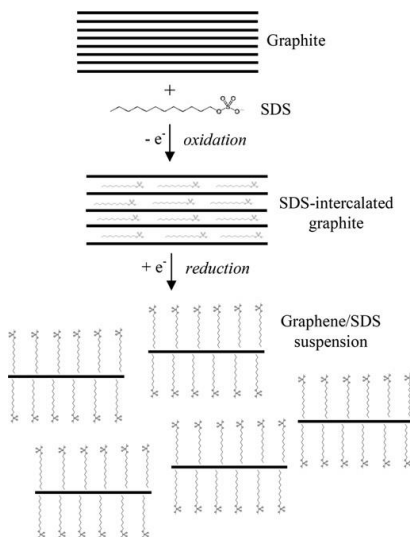


Fig. 1.12 Representative view of electrochemical route to produce graphene/SDS suspension [70].

Alanyaloglu et al. [79] employed a two steps electrochemical route with a three electrodes system for the production of graphene sheets (Fig. 1.12); first

step is the electrochemical intercalation of SDS into graphite and electrochemical exfoliation of a SDS-intercalated graphite electrode is the second one. This two-step process yielded a stable colloidal graphene/SDS suspension.

In the first part of this research, Graphene sheets were produced by electrochemical method and then in the second part of our experiments, we focused on usage and application of the graphene sheets produced by electrochemical way. Recent advances in the bulk production of the exfoliated GSs from graphite bring the possibility of GSs application in the molecular gas sensors [80], energy storage materials [81] and composite materials [82]. Also, the synergistic combination of the high specific surface area and strong nano-filler-matrix adhesion as well as the exceptional mechanical properties of the sp^2 carbon network in GSs [83] improves the mechanical properties of polymer nanocomposites [82]. On the other hand, the electrochemical production of graphene sheets in the presence of a surfactant is known as one of the facile and controllable method for the fabrication of high quality and stable GSs in a large scale.

Graphene can be well dispersed in poly (styrene), poly (acrylonitrile) and poly (methyl methacrylate) matrices and accordingly it improves the Young's modulus and the ultimate strength [84, 91]. For instance, Liang evaluated the molecular-level dispersion of the graphene oxide sheets in PVA matrix and observed a 62% and 76% increase in the young's modulus and tensile strength, respectively [85]. Additionally, Zhao and co-workers reported 150% improvement in the tensile strength and a nearly 10 times increase in Young's modulus of the PVA/GSs nanocomposite loaded by 1.8 vol% GSs [86]. It is worthy of note that in the electrochemical method the re-stacking and agglomeration of the obtained GSs is prevented by the use of surfactants; this results in an

efficient dispersion of GSs which is beneficial in the development of some composites as the reinforcement species [94].

It should be noted that the product of the electrochemical method is a mixture of mono and multilayer GSs and according to Gong and co-workers report, there is a relation between the layer numbers of GSs and reinforcing role of them in polymer matrix. Gong and co-workers have shown that the optimum layer numbers of GSs for reinforcing polymers is related to the polymer layer thickness. According to their results by increasing the polymer layer thickness, maximum composite modulus will obtain by multi-layer GSs (Fig. 1.13) [87].

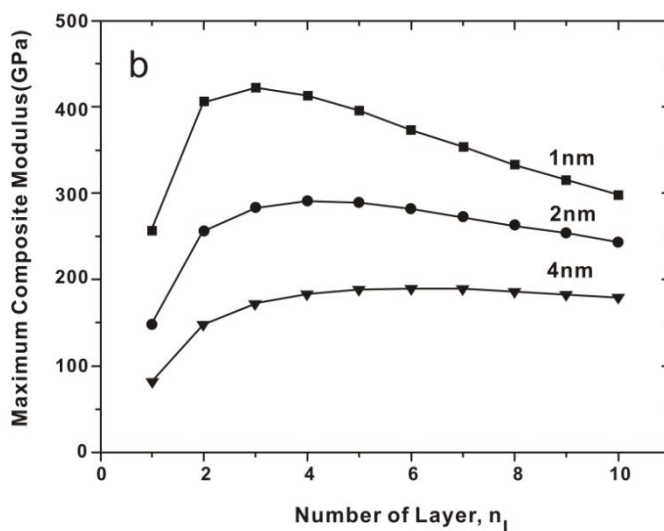


Fig. 1.13 Maximum nanocomposite modulus predicted for different indicated polymer layer thicknesses as a function of the number of layers, n_l , is the number of graphene flakes [87].

In fact, multi-layer SWGSs limit the viscose movement of the polymer chains and improve the elastic movements of them. Thus, for each polymer matrix the gyration radius and its relation with the number of GS's layers should be considered. As a result, it is rational that the SWGSs produced by electrochemi-

cal method be a perfect candidate to improve mechanical properties of the polymers with big gyration radius like PVA.

Chapter 2

Experimental Section

2.1 Experimental Section

2.1.1 Materials

All the reagents used in this study, including graphite plate, SDS, APTES, hydrochloric acid and PVA (with $M_w \approx 72,000$) were provided by Merck and Sigma Aldrich Companies. Deionized water was also used for the preparation of solutions and washing.

2.1.2 Synthesize of the Graphene Sheets

All experiments were conducted in a two-electrode electrochemical cell with working volume of 50mL at 25 °C. A platinum plate and a pure graphite electrode (polished to a mirror finish, washed with acetone and distilled water) were used as the cathode and anode, respectively. The geometric area of the anode and cathode were $1.5 \times 1 \text{ cm}^2$ and $1.5 \times 2 \text{ cm}^2$, respectively. The aqueous electrolyte consisted of 0.1 M SDS with a pH of 8.4 (The reason why we used this concentration is related to the surface tension of liquid, refer to the appendix A). The advantage of SDS, compared to other intercalator such as fluoride [88], nitrate [89], sulfate [90] and lithium [91], is its effective inhibitory role in prevention of re-stacking and agglomeration of the produced layers. However, identification of the role of applied potential in electrochemical intercalation/exfoliation of graphite is a prerequisite for the effective synthesis of graphene sheets [100]. This is especially true when this method have to compete with different chemical/physical based synthesis routes.

The intercalation and exfoliation steps of the graphite plate were performed by applying different potentials of 5, 10, and 15 V for 10 hours. Then, the

obtained stable graphene/SDS suspensions were centrifuged at low speed (5000 rpm) for 20 min. The final samples were exposed to high frequency ultrasonic waves for improving the chemical bonds between graphite layers and SDS; furthermore, the shocks applied by the waves lead to a complete exfoliation of graphite surface [92]. The obtained suspensions were collected with a 200 nm porous filter, washed by DI water and ethanol and then the powders were dried in vacuum oven for 5 hours.

In order to determine SWGSs content of the samples and process efficiency, 20mL of 0.1 M $\text{Ca}(\text{NO}_3)_2$ solution was added to 20 mL graphene/SDS suspension which results in $\text{Ca}(\text{DS})_2$ and SWGSs precipitation. By weighting the filtered samples, SWGSs content and efficiency were estimated [79].

2.1.3 Preparation of SWGSs/PVA Composites

The SWGSs/PVA composites were synthesized in a simple liquid phase blending method. Since, the SWGSs are stable in water and PVA is soluble in water too, this method will result a homogenous mixture simply. A composite film of SWGSs and PVA in different percentage of SWGSs (0.06, 0.1, 0.2, and 0.3 Vol %) was made by drop casting route on a plexiglass substrate and keeping in the vacuum oven at 45 and 60 °C for 24 hours, separately. Consequently, after drying completely, the films were peeled off from the substrate.

2.1.4 Methods of Characterization

In order to preparation of the samples for HRTEM, TEM (JEOL, JEM-2100, operating at 200 kV), FESEM (Mira\\Tescan) and AFM (in tapping mode, Dualscope/Rasterscope C26, DME, Denmark) analyses, APTES was mixed with water and one drop of hydrochloric acid was added; then, Si wafers were entered

into the solution for 30 min and then washed thoroughly with DI water. Afterward, the substrate was dipped in SWGSs solution for 10s and subsequently introduced to the DI water and dried [93]. During the synthesis process, the CTT curves were recorded at different applied potentials. Additionally, in order to study the functionalization of the SWGSs, FT-IR spectra of the graphene dispersion were collected. XRD of the graphene sheets were carried out with Equinox 3000/INEL, France diffractometer with Cu k_{α} radiation ($\lambda = 1.541874\text{\AA}$). In order to study the density of defect and number of SWGSs layers, Raman spectra were recorded with Raman Microprobe Nicolet ALMEGA with 532 nm excitation source under 100 mW power.

To investigate the effect of process temperature on the polymer films, TGA was performed by using of TGA 50 Shimadzu Tokyo Japan with heating rate of 10 °C/min in N₂ atmosphere. Furthermore, DSC was done by Perkin Elmer in a non-isothermal 10 °C/min cooling ramp. The mechanical properties of the nanocomposite sheets with a width of 10 mm were studied with a 5566 U.S.A Instrone at a strain rate of 5 mm/min in ambient situation; in addition, the gauge length in all experiments was 20 mm.

Chapter 3

Results and Discussion

3.1 Result and Discussion

In the electrochemical method there are two fundamental factors which have substantial effects on the quantity and quality of the SWGSs. Firstly, concentration of the electrolyte and secondly, amount of the applied potential.

As we explained in the introduction section about the role of electrolyte concentration in the intercalation and exfoliation phenomena and by considering explanations in the appendix A, 0.1M SDS solution is a good choice to use as the electrolyte [79, 67].

In order to have an exact study on this system, we focused only on one variation; applied potential. Since, SDS molecules in water will be ionized, by applying voltage DS⁻ will be adsorbed on the anode surface (graphite) Fig. 3.1.

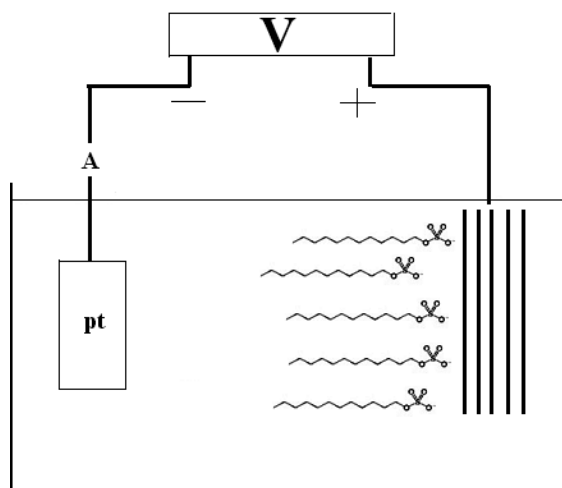


Fig. 3.1 Schematic scheme of intercalation process.

The reaction between graphite (C_x) and DS^- in the solvent (y) can be presented as [79]:



During this reaction, DS^- anions perch among the graphite layers via the formation of π - π chemical bonds with the layers surface which results in the intercalation of graphite [66]. On the other hand, the carbonic chains of DS^- are responsible for the exfoliation of graphite layers. Fig. 3.2 shows a schematic of intercalation and exfoliation of graphite layers.

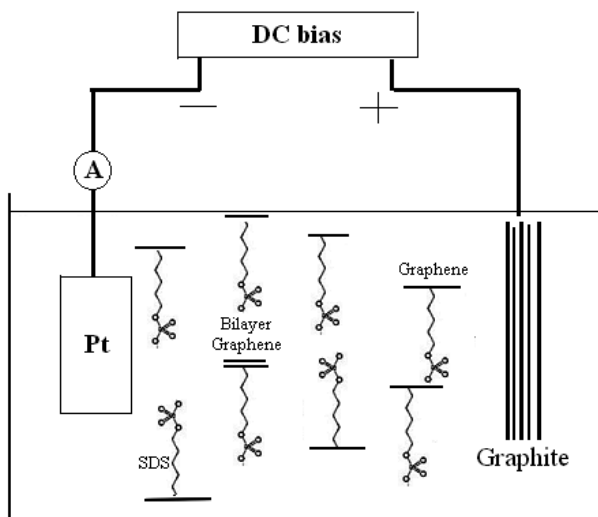


Fig. 3.2 Schematic illustration of the electrochemical and exfoliation of graphite layers to produce SWGSs suspension.

It should be also pointed out again that SDS is an amphiphilic surfactant (with hydrophobic and hydrophilic sections) which results in the stability of prepared SWGSs in the aqueous media.

3.2 Characterization of SWGSs

3.2.1 Chronoamperometry

The transfer of DS^- between graphite layers is a diffusion controlled phenomenon. The CTT curves obtained at different applied potentials (Fig. 3.3) indicates that at initial time of process, the concentration of DS^- at the interface of electrolyte/electrode is high enough and consequently, the diffusion of DS^- into graphite layers is a rapid step (Fick's second law).

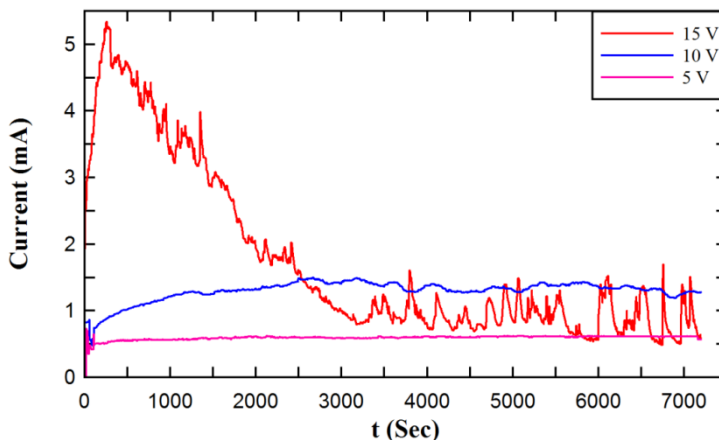


Fig. 3.3 The CCT curves obtained at different potentials in the SWGSs producing.

However, after this initial time, the current drop is inevitable due to an increase in the resistance of electrolyte (limited diffusion). Close observation of Fig. 3.3 shows that at applied potential of 15 V, the efficiency of intercalation step increases as a result of higher electrical driving force; the higher electrical driving force leads to a higher stress applied over the anode compared to other potentials. Regarding the higher rate of solute diffusion at 15 V applied potential, the production yield of high quality SWGSs increases. Under saturation conditions,

the graphite surface is covered by a thin film of SDS which acts as a capacitor; this hinders the diffusion of DS^- and consequently, all CTT curves approach to a constant value after a period (Fig. 3.3). Moreover, the significant fluctuations observed in the CTT curve corresponding to 15 V can be attributed to higher electrical driving force; i.e. the high driving force leads to repetitive exfoliation of SWGSs over the graphite surface and results in the formation of fresh surface during the electrochemical process [100, 94].

Another evidence for the repetitive exfoliation of SWGSs is the color of graphene/SDS suspension prepared at different applied potentials; the higher level of applied potential results in the darker color of samples (Fig. 3.4) which can be attributed to higher level of exfoliated graphite present in the solution [100, 66].

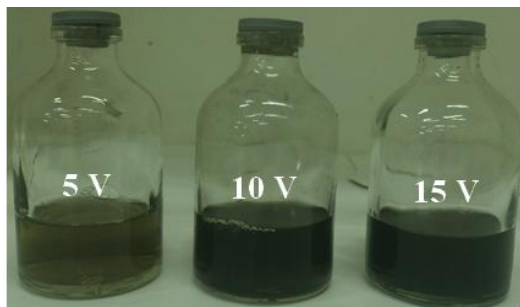


Fig. 3.4 Image of the prepared samples in different applied potentials.

The estimated amounts of SWGSs are 11.3, 7.65 and 5 g/L for 15, 10 and 5 V potentials, respectively; these results are in good agreement with chronoamperometry analysis.

3.2.2 Raman Spectroscopy

Fig. 3.5 shows the Raman spectra of SWGSs obtained at different applied potentials.

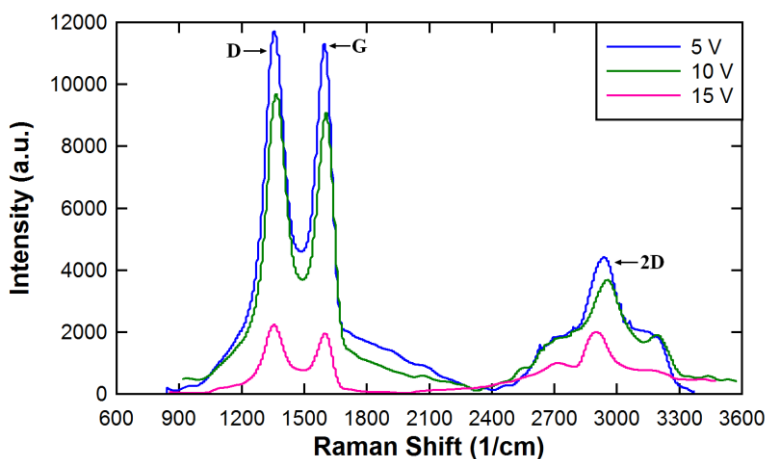


Fig. 3.5 Raman spectra of the obtained SWGSs in different applied potentials.

The presence of D, 2D and G peaks [95] in all spectra confirms the formation of SWGSs in all conditions. Regarding the fact that the lower number of graphene layers results in narrower 2D peak with red shifts [94], it can be concluded that an increase in the level of applied potential leads to the formation of lower number of graphene layers [96]. However, the shape and frequency of 2D peak are affected by the layer numbers of GSs [95, 34]. The 2D band of the monolayer GSs appears at 2679 cm^{-1} , while the 2D peak of 2-4 layers shifts to 2798 cm^{-1} ($+19\text{ cm}^{-1}$) [95]. Regarding the Raman spectra presented in Fig. 3.5, the appearance of 2D peak at 2698 cm^{-1} confirms the formation of 2-4 layers SWGSs. However, since 2D peak in the spectrum corresponding to 15 V is neither sharp nor symmetric, it is most likely that a mixture of monolayer and multilayer SWGSs has been obtained under these

conditions. Another important point regarding graphene layer thickness is the intensity of G band [96]. It is worthy of note that the peak corresponding to the G band of the single layer of graphene occurs at $\sim 1585 \text{ cm}^{-1}$ and the shift in the position of the G band $\sim -6 \text{ cm}^{-1}$, is due to the stacking 2-6 layers [97]. According to the Fig. 3.5 the observed peak at $\sim 1580 \text{ cm}^{-1}$ can be also assigned to the presence of a mixture of monolayers and multilayer SWGSs. Close observation of Fig. 3.5 reveals that the SWGSs obtained at 15 V have minimum number of the layers.

The defects percentage of the obtained SWGSs at different applied potentials can be estimated using [98, 99]:

$$X_G = \frac{I_G}{I_G + I_D}, X_D = 1 - X_G \quad \text{Eq. 3.2}$$

Where X_G and X_D are the molar fraction of carbon atoms with regular and irregular SP^2 bond, respectively. Also, I_G and I_D are the intensity of G and D peaks appeared in Raman spectrum. The results of this exercise indicates that the amount of carbon with regular SP^2 bond slightly decreases by increasing applied potentials which is due to the more interactions between GSs and SDS molecules and partial oxidation of the SWGSs at the higher applied potential. Also, the broadness of the peaks observed in the Raman spectra (Fig. 3.5) indicates the presence of highly functionalized SWGSs due to the strong interactions between SDS molecules and GSs [100].

3.2.3 FT-IR Analysis

FT-IR spectrum of the SWGSs produced at 15 V has been shown in Fig. 3.6. It is worthy of note that in this FT-IR spectrum, prominent features corresponding to graphene oxide, including absorption bands corresponding to C–O stretching at

1053 cm^{-1} , phenolic O–H deformation vibration at 1412 cm^{-1} , C = C ring stretching at 1621 cm^{-1} , C=O carbonyl stretching at 1733 cm^{-1} , are not present [101]. However, the characteristic stretching bands at 3485 and 1224 cm^{-1} corresponding to OH and C-OH [102] indicate partial oxidation of the SWGSs during exfoliation/dispersion step [68]. Also, the stretching bands of the C-H functional groups as well as the C-H vibration band appear at 2920, 2850 and at 1470 cm^{-1} , respectively [66].

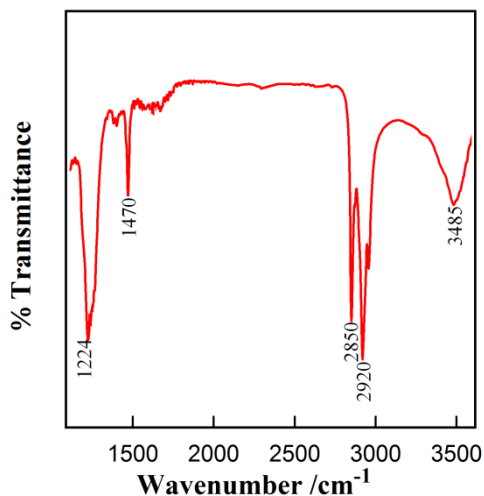


Fig. 3.6 FT-IR spectra of SWGSs produced at 15 V.

3.2.4 AFM Result

According to the AFM image presented in Fig. 3.7, the thickness of the thinnest SWGSs obtained at 15 V is estimated around 1.87 nm.

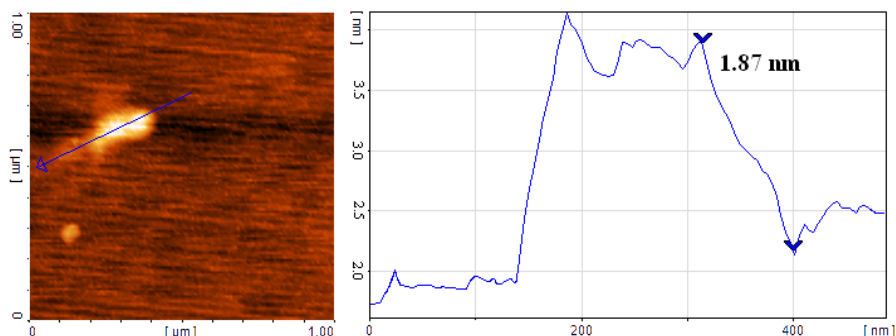


Fig. 3.7 AFM image of prepared SWGSs in applied 15V.

Regarding the thickness of pristine GS (~ 0.34 nm), it can be concluded that SWGSs consist of 1–3 layers of GS [34]. It should be pointed out that the presence of solvent/SDS molecules, oxidized parts and functionalized groups in the SWGS as well as crumpling and scrolling of the SWGS due to thermal fluctuations can result in the overestimation of thickness via AFM [66]. The circular shape of the obtained SWGSs (Fig. 3.7), which appears as a result of solution treatment and formation of nanoparticles colloid, is due to achieving minimum surface area. On the other hand, high speed centrifugation results in the agglomeration of some SWGSs [79].

3.2.5 X-Ray Diffraction

In Fig. 3.8, the XRD patterns corresponding to the graphite and electrochemically synthesized graphene at 15 V are presented.

As it can be observed, a high percentage of graphite layers have been converted to SWGSs after the synthesis process; the sharp peak at $2\theta = 26$ related to (002) graphite disappears in the XRD pattern of graphene. Moreover, the peak broadening from $2\theta = 12.7$ to 40 indicates the presence of different number of graphene layers [79, 103].

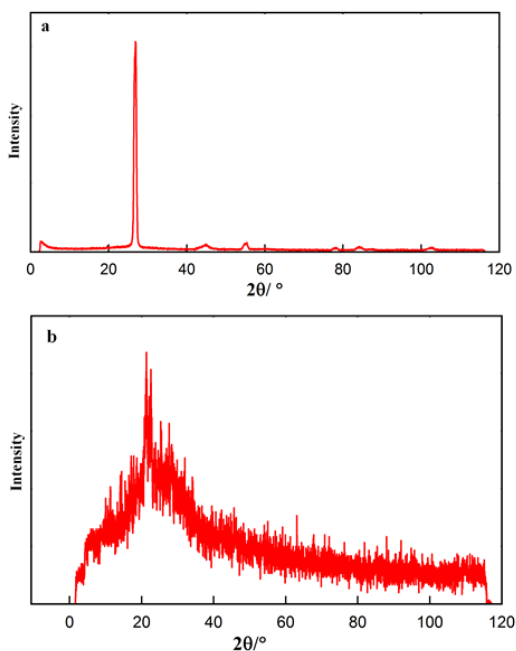


Fig. 3.8 XRD patterns of (a) raw graphite and (b) SWGSs produced at 15 V.

3.2.6 Electron Microscopic Studies

Fig. 3.9 shows the FESEM images of SWGSs obtained at 15 V. It is worthy of note that the majority of waves observed in graphene sheet structure are transparent (Fig. 3.9 a). Also, the buckling/wrinkling appeared in some SWGSs is due to thermodynamic stability of 2D structure of graphene [34].

The transparency and thickness of multilayers SWGSs were evaluated using TEM. Fig. 3.10 shows both the monolayer and multilayers SWGSs (black arrays).

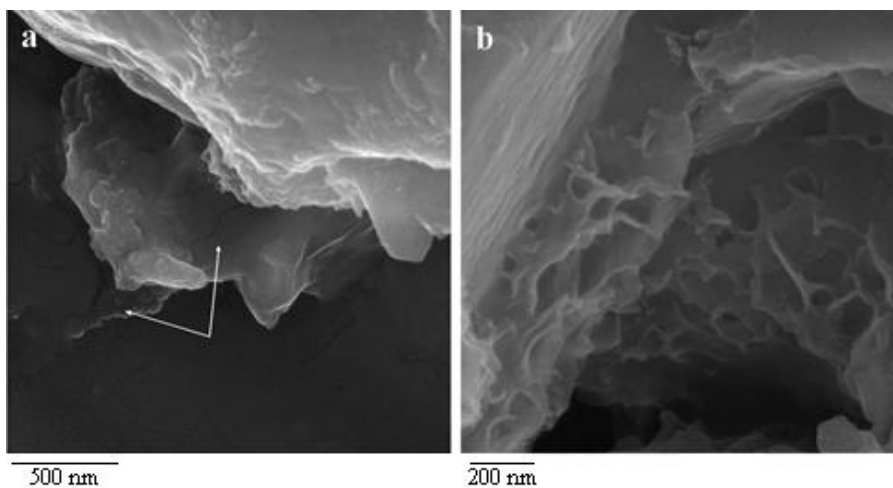


Fig. 3.9 FESEM images of the synthesized SWGSs at 15 V.

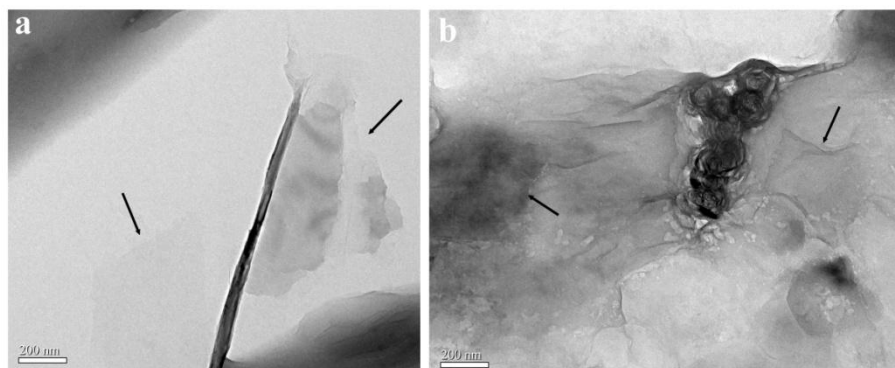


Fig. 3.10 TEM images of the synthesized SWGSs at 15 V.

Additionally, the interlayer distance of SWGSs is estimated around 0.34 nm based on HRTEM observation (Fig. 3.11), which is in agreement with the bilayer distance of graphite planes [113].

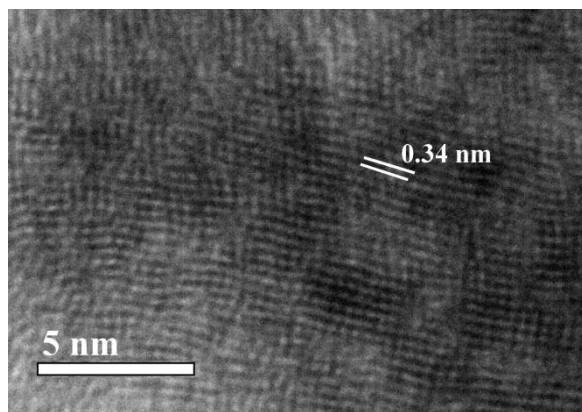


Fig. 3.11 HRTEM image of the interlayer distance in synthesized SWGSs at 15 V.

Also, the synergistic combination of the high specific surface area and strong nano-filler-matrix adhesion as well as the exceptional mechanical properties of the sp^2 carbon network in GSs [91] improves the mechanical properties of polymer nanocomposites [82, 84]. On the other hand, the electrochemical production of SWGSs in the presence of a surfactant is known as one of the facile and controllable method for the fabrication of high quality GSs in a large scale.

3.3 Characterization of SWGSs/PVA Nanocomposite Films

3.3.1 XRD Patterns

In order to assess the structure, crystallinity percentage and interlayer changes of the fabricated nanocomposites, XRD was carried out. The sharp peak around $2\theta=19.4$ (d-spacing of 0.45 nm) and the feeble bulge appeared at $2\theta=40.4$ (d-spacing of 0.22 nm) (Fig. 3.12) are assigned to the semi-partial crystalline structure of PVA [68]. Also, the disappearance of the broad peak

corresponding to SWGSs is contributed to molecular level dispersion of SWGSs in PVA matrix resulted in loss of structure regularity of SWGSs [86]. As can be observed, the (101) peak is intensified at the higher level of SWGSs in the polymer matrix which is contributed to an increase in the number of PVA chains packing. In fact, the SWGSs act as the nucleating agents and accordingly, the crystallinity of the composites improves.

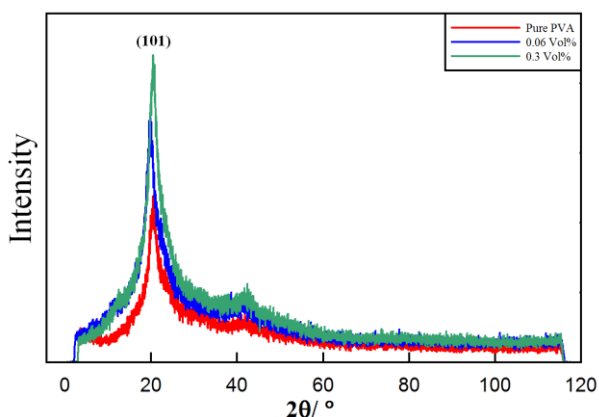


Fig. 3.12 XRD patterns of SWGSs/PVA nanocomposit with various graphene contents.

3.3.2 Mechanical Properties

As it has been mentioned previously, to have maximum composite modulus the relation between number of GSs for reinforcing polymers and the polymer layer thickness should be taken in account. Thus, about the PVA [104] multi-layer SWGSs can obtain the maximal mechanical properties of the nanocomposites. In Fig. 3.13 the column curves of the mechanical properties of the prepared composite films at 45 and 60 °C with various SWGSs loading are presented.

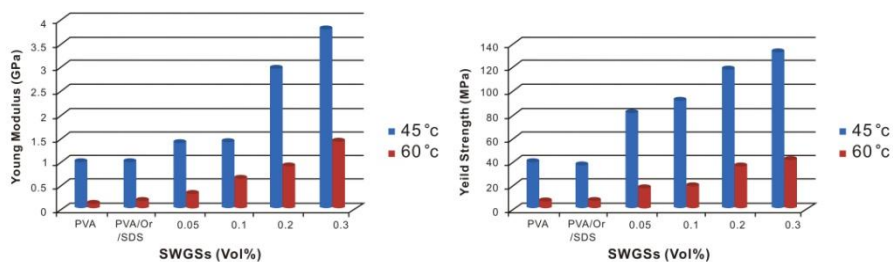


Fig. 3.13 Comparison between mechanical properties of the prepared samples at 45 and 60 °C.

As it can be observed, the strength and young’s modulus of the nanocomposites increase by increasing the percentage of the SWGSs. The physicochemical interactions between the pendant hydroxyl groups of PVA with SDS molecules accompanied by GSs (hydrogen bonding) [105], result in improvement of the nanocomposite films’ mechanical properties even at low loading SWGSs.

According to Fig. 3.14, the nanocomposites reach a mechanical percolation point (0.2 and 0.1 Vol% SWGSs for the nanocomposites prepared at 45 and 60 °C, respectively).

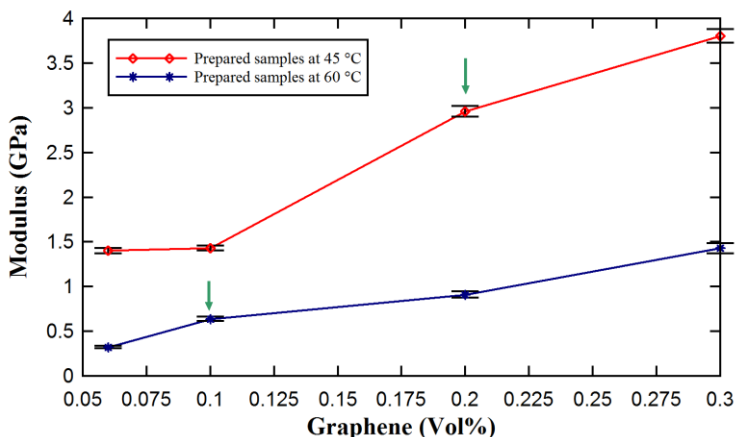


Fig. 3.14 Young’s modulus of the nanocomposite films versus SWGSs loadings.

At the percolation point, there is a long-range interaction between random chains of PVA and SWGSs. In fact at this point, the chains of the PVA and SWGSs form a 3D structure and consequently, the chains of polymer cannot move easily [86]; i.e. the mechanical properties of the nanocomposites are enhanced. The main and distinctive point between the obtained results with previous works [82, 91, 86, 105, 106, 107] is the low level of SWGSs used for the fabrication of the nanocomposites; i.e. the uniform distribution of the reinforcements in polymer matrix [107, 86] is achieved by adding only 0.2 and 0.1 Vol % SWGSs in the nanocomposites prepared at 45 and 60 °C.

It is remarkable that the prepared nanocomposite films at 45 °C show yielding points in their stress-strain curve, while, the produced films at 60 °C do not have yielding point and their strength increase uniformly till fracture point (Fig. 3.15).

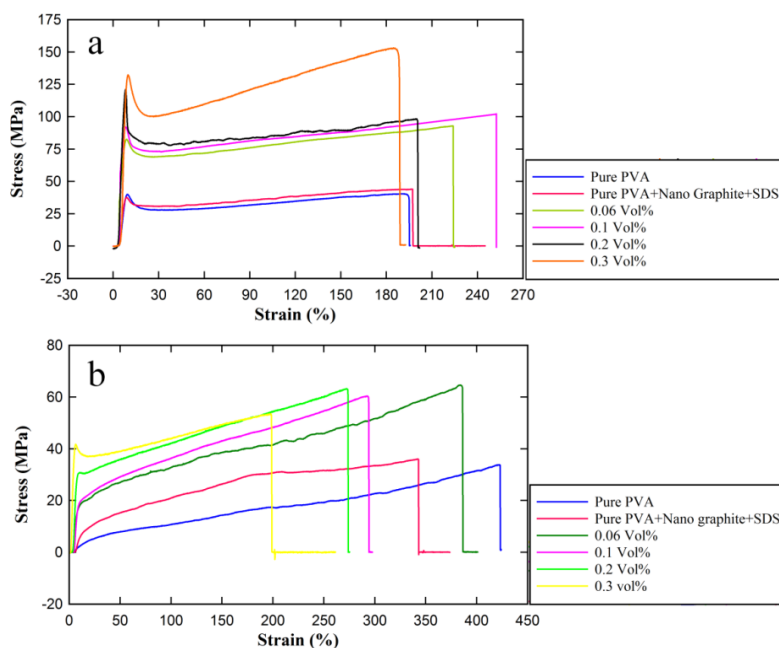


Fig. 3.15 The stress-strain curves of SWGSs/PVA nanocomposite films (a) at 45 °C and (b) 60 °C.

3.3.3 Thermal Studies

In order to study the effect of SWGSs on the dynamic crystallization of PVA and the macroscopic properties of the nanocomposite films, DSC was conducted. As it is shown in table 3.1, the T_p gradually increases by increasing the graphene loading level; this reveals that the SWGSs act as seeds for the faster nucleation (confirmation the XRD results in 3.3.1 sec.) [108].

Table 3.1 *The percent of crystallinity and T_p of the nanocomposite films.*

Samples	Crystallinity (%)	T_p
Pure PVA at 45°C	17.2	191.2
Pure PVA at 60°C	16.07	188.4
0.2 % Vol at 45°C	20.2	193.1
0.1% Vol at 60°C	25.24	194.7

The crystallinity of PVA and the nanocomposites can be calculated by using of the DSC analyze (the enthalpy of 100% crystallinity of PVA is 138.6 J/g [109, 110]). By considering the weight fraction of PVA in the nanocomposite films, the crystallinity of PVA is determined.

Thus, the significant improvement in the mechanical properties of the nanocomposites stems from the presence of these crystalline shells which creates an effective attachment of PVA to the nanosheets of SWGSs that constrains the segmental motion of the polymer chains [105].

According to the results given in table 3.1, in the presence of SWGSs, the variation in the crystallinity percentages of the samples prepared at 60 °C is higher than that of at 45 °C; thus, the higher number of crystals at 60 °C results in the stacking the polymeric chains and accordingly, the elongation percentage reduces at higher level of reinforcement [108]. On the other hand, for the samples prepared at 45 °C, SDS molecules play the role a plasticizer.

It should be noted that the drying process of the nanocomposites was conducted from ambient temperature up to 45 and 60 °C. At the higher temperature range (ambient temperature to 60 °C), the movement of polymer chains is more than other sample; i.e. the structural order becomes lower at the higher temperature. Since, the time of drying process was set the same for both nanocomposite films, it can be concluded that the crystallinity percentage of samples that were dried in the range of ambient temperature to 45 °C, is higher.

An interesting point regarding the mechanical properties is that the percolation point corresponding to the sample prepared at lower temperature range (ambient temperature to 45 °C) occurs at 0.2 Vol % of SWGSs; while, for sample dried at higher temperature range, the percolation point is at 0.1 Vol % of SWGSs. The higher volume percentage of the SWGSs in the former case is another reason for the more crystallinity percentage of these samples.

For further evaluation, the TGA curves corresponding to the pure PVA films [84, 111, 112] are presented in Fig. 3.16.

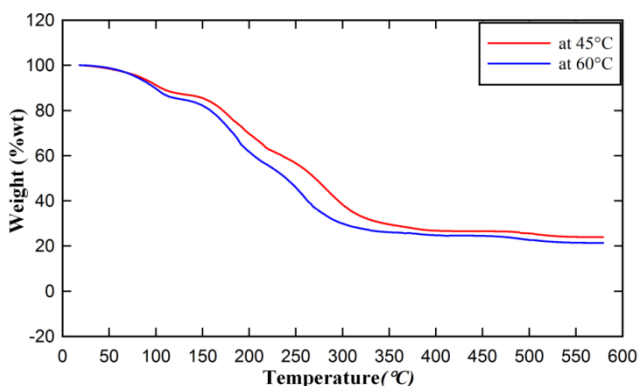


Fig. 3.16 TGA curves of the pure PVA films at 45 and 60 °C.

As it can be seen, the percentage of weight loss and decomposition rate for the sample prepared at 60 °C is higher than the sample prepared at 45 °C. Thus,

mobility of the SDS and polymer chains is higher in prepared samples at 60 °C and accordingly, there is less grafting between chains compared to the prepared films at 45 °C; so, a higher elongation and lower strength is observed in the case of nanocomposite prepared at 60 °C compared to that at 45 °C.

A comparison between the thermal and the mechanical properties of the pure PVA and SWGSs/PVA nanocomposites at the percolation threshold indicates that the SWGSs can effectively reduce the effect of degradation of the PVA during the synthesis process of nanocomposites (synergetic effect). Consequently, the yielding point of the nanocomposites shifts to the higher percentages of SWGSs for the prepared samples at 60 °C.

3.3.4 FE-SEM Studies

According to the FE-SEM images of the fracture surface of the nanocomposite films (Fig. 3.17) at their percolation points, layered-structures with fully exfoliated and well-dispersed SWGSs in the PVA matrix with the lowest amount of restacking the nanosheets compared to the pure PVA were revealed [105]. Furthermore, the images show that the SWGSs are distributed in a 3D network in the polymer matrix [86].

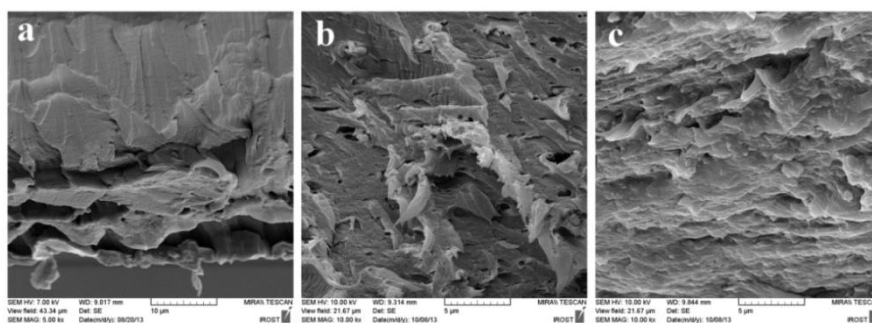


Fig. 3.17 The FE-SEM images of the (a) pure PVA, nanocomposite films prepared at (b) 45 °C with 0.2 Vol% SWGSs, and (c) 60 °C with 0.1 Vol %.

Conclusion

In this work, SWGSs were successfully prepared in a double electrodes cell in the presence of SDS. The role of applied potential on the formation of the SWGSs was clarified. According to the CCT curves, higher electrical driving force resulted in more efficient intercalation/exfoliation steps; an increase in the level of applied potential (5-15 V), the efficiency of SWGSs production increases to 56%. Characterization of the obtained SWGSs at 15 V confirmed low defect density with thinnest thickness of 1.87 nm (700 nm width) indicating the presence of a mixture of GSs with various numbers of layers of the product. The SWGSs prepared via this method was stable in water for 6 months; this promising characteristic makes it as a potential candidate for the fabrication of nanocomposites based polymer (PVA). In the second step of the work, we synthesized the PVA/SWGSs nanocomposite films via liquid blending method. Surprisingly, the mechanical properties of the nanocomposite films in the present of low content SWGSs showed a notable improvement which it is related to well distribution of the multilayer SWGSs in the matrix and strong interactions between them and polymer chains. Furthermore, in order to more study the mechanical properties of the films, the thermal investigations were carried out. The presence of crystalline shells in the nanocomposites is responsible for the improvement of the mechanical properties. According to the thermal analyses results SWGSs in the prepared samples at 60 °C have the synergetic effect; it means that as well as the reinforcement role, they compensate the higher rate of decomposition samples at higher temperature and it is the origin of the differences in their stress-strain curves.

References

- [1] K. S. Novoselov, A. K. Geim, S. V. Morozov, D. Jiang, Y. Zhang, S. V. Dubonos, I. V. Grigorieva, A. A. Firsov, "Electric field effect in atomically thin carbon films", *Science*, vol. 306, pp. 666-669, 2004.
- [2] www.intechopen.com, "*Functionalization of Carbon Nanotubes*", D. S. Yellampalli, Ed., Publisher InTech, 2011.
- [3] W. J. Cantwell, J. Morton, "The impact resistance of composite materials", *Composites*, vol. 22, pp. 347-362, 1991.
- [4] A. K. Geim, "Graphene: Status and Prospects", *Science*, vol. 324, pp. 1530-1534, 2009.
- [5] A. H. Castro Neto, F. Guinea, N. M. R. Peres, K. S. Novoselov, and A. K. Geim, "The electronic properties of graphene", *Reviews of Modern Physics*, vol. 81, p. 109-161, 2009.
- [6] H. P. Boehm, R. Setton, E. Stumpp, "Nomenclature and terminology of graphite intercalation compounds", *Pure Appl. Chem.*, vol. 66, p. 1893-1901, 1994.
- [7] R. Saito, M. S. Dresselhaus, G. Dresselhaus, "*Physical Properties of Carbon Nanotubes*", Imperial College, 1998.
- [8] A. K. Geim, K. S. Novoselov, "The rise of graphene", *Nat. Mater.*, vol. 6, pp. 183-191, 2007.
- [9] P. R. Wallace, "The band theory of graphite", *Phys. Rev.*, vol. 71, p. 622-634, 1947.
- [10] G. S. Painter and D. E. Ellis, "Electronic band structure and optical properties of graphite from a variational approach", *Phys. Rev. B*, vol. 1, p. 4747-4752, 1970.
- [11] L. D. Landau, "Zur Theorie der Phasenumwandlungen II", *Phys. Z. Sowjetunion*, vol. 11, p. 2635. 3.
- [12] J. M. Blakely, J. S. Kim, H. C. Potter, "Segregation of Carbon to the (100) Surface of Nickel", *J. Appl. Phys.*, vol. 41, pp. 2693-2697, 1970.

References

- [13] M. Eizenberg, J. M. Blakely, "Carbon interaction with nickel surfaces: Monolayer formation and structural stability", *J. Chem. Phys.*, vol. 71, p. 3467, 1979.
- [14] J. C. Hamilton, J. M. Blakely, "Carbon layer formation on the Pt (111) surface as a function of temperature", *J. Vac. Sci. Tech.*, vol. 15, pp. 559-562, 1978.
- [15] A. J. Van Bommel, J. E. Crombeen, A. Van Tooren, "LEED and Auger Electron Observations of the SiC(0001) Surface", *Surface Science*, vol. 48, p. 463-472, 1975.
- [16] W. S. Hummers Jr., R. E. Offeman, "Preparation of Graphitic Oxide", *J. Am. Chem. Soc.*, vol. 80, p. 1339, 1958.
- [17] D. R. Dreyer, R. S. Ruoff, C. W. Bielawski, "From Conception to Realization: An Historical Account of Graphene and Some Perspectives for Its Future", *Angewandte Chemie International Edition*, vol. 49, p. 9336-9344, 2010.
- [18] F. J. Himpsel, K. Christmann, P. Heimann, D. E. Eastman, P. J. Feibelman, "Adsorbate band dispersions for C on Ru(0001)", *Surface Science*, vol. 115, p. 159-164, 1982.
- [19] R. Rosei, M. De Crescenzi, F. Sette, C. Quaresima, A. Savoia, and P. Perfetti, "Structure of graphitic carbon on Ni(111): A surface extended-energy-loss finestructure study", *Phys. Rev. B*, vol. 28, p. 1161-1164, 1983.
- [20] K. S. Novoselov¹, A. K. Geim¹, S. V. Morozov, D. Jiang, M. I. Katsnelson, I. V. Grigorieva, S. V. Dubonos, A. A. Firsov, "Two-dimensional gas of massless Dirac fermions in graphene", *nature*, vol. 438, pp. 197-200, 2005.
- [21] K. S. Novoselov, Z. Jiang, Y. Zhang, S. V. Morozov, H. L. Stormer, U. Zeitler, J. C. Maan, G. S. Boebinger, P. Kim, A. K. Geim, "Room-temperature quantum Hall effect in graphene", *Science*, vol. 438, p. 1379, 2007.
- [22] Y. Zhang, Y. W. Tan, H. L. Stormer, P. Kim, "Experimental observation of the quantum Hall effect and Berry's phase in graphene", *nature*, vol. 438, pp. 201-204, 2005.
- [23] Claire Berger, Zhimin Song, Tianbo Li, Xuebin Li, Asmerom Y. Ogbazghi, Rui Feng, Zhenting Dai, Alexei N. Marchenkov, Edward H. Conrad, Phillip N. First, Walt A. de Heer, "Ultrathin Epitaxial Graphite: 2D Electron Gas

- Properties and a Route toward Graphene-based Nanoelectronics”, *J. Phys. Chem. B.*, vol. 108, pp. 19912-19916, 2004.
- [24] Changgu Lee, Xiaoding Wei, Jeffrey W. Kysar, James Hone, “Measurement of the Elastic Properties and Intrinsic Strength of Monolayer Graphene”, *Science*, vol. 321, pp. 385-388, 2008.
- [25] Alexander A. Balandin, Suchismita Ghosh, Wenzhong Bao, Irene Calizo, Desalegne Teweldebrhan, Feng Miao, Chun Ning Lau, “Superior Thermal Conductivity of Single-Layer Graphene”, *Nano Lett.*, vol. 8, pp. 902-907, 2008.
- [26] K. I. Bolotin, K. J. Sikes, Z. Jiang, M. Klima, G. Fudenberg, J. Hone, P. Kim, H. L. Stormer, “Ultrahigh electron mobility in suspended graphene”, *Solid State Commun.*, vol. 146, pp. 351-355, 2008.
- [27] M. D. Stoller, S. Park, Y. Zhu, J. An, R. S. Ruoff, “Graphene-Based Ultracapacitors”, *Nano Lett.*, vol. 8, p. 3498-3502, 2008.
- [28] P. Blake, E. W. Hill, A. H. Castro Neto, K. S. Novoselov, D. Jiang, R. Yang, T. J. Booth, A. K. Geim, “Making graphene visible”, *Applied Physics Letters*, 063124, vol. 91, pp. 063124-3, 2007.
- [29] R. H. Savage, “Graphite lubrication”, *Journal of Applied Physics*, vol. 19, pp. 1-10, 1948.
- [30] A. Pertsin, M. Grunze1, “Water as a lubricant for graphite: a computer simulation study”, *J Chem Phys.*, vol. 125, p. 114707, 2006.
- [31] Gertjan S. Verhoeven, Martin Dienwiebel, Joost W. M. Frenken, “Model calculations of superlubricity of graphite”, *Phys. Rev. B.*, vol. 70, p. 165418, 2004.
- [32] Quanshui Zheng, Bo Jiang, Shoupeng Liu, Yuxiang Weng, Li Lu, Qikun Xue, Jing Zhu, Qing Jiang, Sheng Wang, Lianmao Peng, “Self-Retracting Motion of Graphite Microflakes”, *Phys. Rev. Lett.*, vol. 100, p. 067205, 2008.
- [33] I. W. Frank, D. M. Tanenbaum, A. M. van der Zande and P. L. McEuen, “Mechanical properties of suspended graphene sheets”, *J. Vac. Sci. Technol. B.*, vol. 25, pp. 2558-2561, 2007.

References

- [34] M. I. Katsnelson, K. S. Novoselov, T. J. Booth, S. Roth, Jannik C. Meyer, A. K. Geim, "The structure of suspended graphene nanosheets", *Nature*, vol. 446, p. 60-63, 2007.
- [35] Y. Zhang, J. P. Small, W. V. Pontius, P. Kim, "Fabrication and electric-field-dependent transport measurements of mesoscopic graphite devices", *Applied Physics Letters*, vol. 86, p. 073104, 2005.
- [36] M. Ishigami, J. H. Chen, W. G. Cullen, M. S. Fuhrer and E. D. Williams, "Atomic Structure of Graphene on SiO₂", *Nano Lett.*, vol. 7, pp. 1643-1648, 2007.
- [37] J. Moser, A. Barreiro and A. Bachtold, "Current-induced cleaning of graphene", *Appl. Phys. Lett.*, vol. 91, p. 163513, 2007.
- [38] X. Liang, Z. Fu, S. Y. Chou, "Graphene Transistors Fabricated via Transfer-Printing In Device Active-Areas on Large Wafer", *Nano Lett.*, vol. 7, pp. 3840-3844, 2007.
- [39] I. Forbeaux, J. Themlin and Debever, "High-temperature graphitization of the 6H-SiC (000(1) over-bar) face", *J. Surf. Sci.*, vol. 442, pp. 9-18, 1999.
- [40] G. M. Rutter, J. N. Crain, N. P. Guisinger, T. Li, P. N. First, J. A. Stroscio, "Scattering and interference in epitaxial graphene", *Science*, vol. 317, p. 219-222, 2007.
- [41] P. Sutter, "Epitaxial graphene: How silicon leaves the scene", *Nat. Mater.*, vol. 8, pp. 171-172, 2009.
- [42] J. Hass, R. Feng, T. Li, X. Li, Z. Zong, W. A. de Heer, P. N. First, E. H. Conrad, C. A. Jeffrey and C. Berger, "Highly-ordered graphene for two dimensional electronics", *Appl. Phys. Lett.*, vol. 89, p. 143106, 2006.
- [43] K. V. Emtsev, A. Bostwick, K. Horn, J. Jobst and G. L. e. a. Kellogg, "Towards wafer-size graphene layers by atmospheric pressure graphitization of silicon carbide", *Nat. Mater.*, vol. 8, p. 203-207, 2009.
- [44] S. Bae, H. Kim, Y. Lee, X. Xu, J.-S. Park, Y. Zheng, J. Balakrishnan, T. Lei, H. R. Kim, Y. Song, Y.-J. Kim, K. S. Kim, B. Özyilmaz, J.-H. Ahn, B. H. Hong, S. Iijima, "Roll-to-roll production of 30-inch graphene films for transparent electrodes", *Nat. Nanotechnol.*, vol. 5, pp. 574-578, 2010.

- [45] X. Li, W. Cai, J. An, S. Kim, J. Nah, D. Yang, R. Piner, A. Velamakanni, I. Jung, E. Tutuc, S. K. Banerjee, L. Colombo, R. S. Ruoff, "Large-area synthesis of high-quality and uniform graphene films on copper foils", *Science*, vol. 324, pp. 1312-1314, 2009.
- [46] C. Soldano, A. Mahmood and E. Dujardin, "Production, properties and potential of graphene", *Carbon*, vol. 48, pp. 2127-2150, 2010.
- [47] C. Mattevi, H. Kim, M. Chhowalla, "A review of chemical vapour deposition of graphene on copper", *J. Mater. Chem.*, vol. 21, p. 3324-3334, 2011.
- [48] M. Congqin, Z. Churan, L. Owen and X. Ya-Hong, "*Chemical Vapor Deposition of Graphene. In Physics and Applications of Graphene*", InTech: Rijeka, pp. 37-54, 2011.
- [49] H. Kim, C. Mattevi, M. R. Calvo, J. C. Oberg, L. Artiglia, S. Agnoli, C. F. Hirjibehedin, M. Chhowalla, E. Saiz, "Activation Energy Paths for Graphene Nucleation and Growth on Cu", *ACS Nano*, vol. 6, pp. 3614-3623, 2012.
- [50] K Kim, Z Lee, W Regan, C Kisielowski, MF Crommie, A Zettl, "Grain boundary mapping in polycrystalline graphene", *ACS Nano*, vol. 5, pp. 2142-2146, 2011.
- [51] Q. Yu, L. A. Jauregui, W. Wu, R. Colby, J. Tian, Z. Su, H. Cao, Z. Liu, D. Pandey, D. Wei, T. F. Chung, P. Peng, N. P. Guisinger, E. A. Stach, J. Bao, S.-S. Pei, Y. P. Chen, "Control and characterization of individual grains and grain boundaries in graphene grown by chemical vapour deposition", *Nat. Mater.* 10, 443., vol. 10, pp. 443-449, 2011.
- [52] T. Yoon, W. C. Shin, T. Y. Kim, J. H. Mun, T.-S. Kim and B. Cho, "Direct measurement of adhesion energy of monolayer graphene as-grown on copper and its application to renewable transfer process.", *Nano Lett.*, vol. 12, p. 1448-1452, 2012.
- [53] Z. Sun, Z. Yan, J. Yao, E. Beitler, Y. Zhu and J. M. Tour, "Growth of graphene from solid carbon sources", *Nature*, vol. 468, pp. 549-452, 2010.
- [54] H. Ji, Y. Hao, Y. Ren, M. Charlton, W. H. Lee, Q. Wu, H. Li, Y. Zhu, Y. Wu, R. Piner, R. S. Ruoff, "Graphene growth using a solid carbon feedstock and hydrogen.", *ACS Nano.*, vol. 5, p. 7656-7661, 2011.

References

- [55] Z. Yan, Z. Peng, Z. Sun, J. Yao, Y. Zhu, Z. Liu, P. M. Ajayan, J. M. Tour, "Growth of bilayer graphene on insulating substrates", *ACS nano*, vol. 5, pp. 8187-8192, 2011.
- [56] L. M. A. Perdigão, S. N. Sabki, J. M. Garfitt, P. Capiod, P. H. Beton, "Graphene Formation by Decomposition of C60", *J. Phys. Chem. C*, vol. 115, p. 7472-7476, 2011.
- [57] H.-J. Shin, W. M. Choi, S.-M. Yoon, G. H. Han, Y. S. Woo, E. S. Kim, S. J. Chae, X.-S. Li, A. Benayad, D. D. Loc, F. Gunes, Y. H. Lee, J.-Y. Choi, "Transfer-free growth of few-layer graphene by self-assembled monolayers.", *Adv Mater.*, vol. 23, p. 4392-4397, 2011.
- [58] S. Vadukumpully, J. Paul, S. Valiyaveetil, "Cationic surfactant mediated exfoliation of graphite into graphene flakes", *Carbon*, vol. 47, pp. 3288-3294, 2009.
- [59] Li X, X. Wang, L. Zhang, S. Lee, H. Dai, "Chemically Derived, Ultrasoft Graphene Nanoribbon Semiconductors", *Science*, vol. 319, pp. 1229-1232, 2008.
- [60] S. Park, R. S. Ruoff, "Chemical methods for the production of graphenes.", *Nat. Nanotechnol.*, vol. 4, pp. 217-224, 2009.
- [61] D. C. Schafhaeutil, "Ueber die Verbindungen des Kohlenstoffes mit Silicium, Eisen und anderen Metallen, welche die verschiedenen Gallungen von Roheisen, Stahl und Schmiedeeisen bilden", *Issue Journal für Praktische Chemie*, vol. 21, pp. 129-157, 1840.
- [62] D. R. Dreyer, S. Park, C. W. Bielawski, R. S. Ruoff, "The chemistry of graphene oxide", *Chem. Soc. Rev.*, vol. 39, pp. 228-240, 2010.
- [63] D. Chen, X. Zhao, S. Chen, H. Li, X. Fu, Q. Wu, S. Li, Y. Li and e. al., "One-Pot Fabrication of FePt/Reduced Graphene Oxide composites as Highly Active and Stable Electrocatalysts for the Oxygen Reduction", *Carbon*, vol. 68, pp. 755-762, 2014.
- [64] A. B. Kaiser, C. Gómez-Navarro, R. S. Sundaram, M. Burghard, K. Kern, "Electrical Conduction Mechanism in Chemically Derived Graphene Monolayers", *Nano letter*, vol. 9, pp. 1787-1792, 2009.

- [65] R. Y. N, Gengler, K. Spyrou, P. Rudolf, "A roadmap to high quality chemically prepared graphene", *J. Phys. D: Appl. Phys.*, vol. 43, pp. 1-19, 2010.
- [66] N. Liu, F. Luo, H. Wu, Y. Liu, C. Zhang, J. Chen, "One-Step Ionic-Liquid-Assisted Electrochemical Synthesis of Ionic-Liquid-Functionalized Graphene Sheets Directly from Graphite", *Adv. Funct. Mater.*, vol. 18, p. 1518-1525, 2008.
- [67] Y. Hernandez, V. Nicolosi, M. Lotya, F. M. Blighe, Z. Sun, S. De, I. T. McGovern, B. Holland, M. Byrne, Y. K. Gun'Ko, J. J. Boland, P. Niraj, G. Duesberg, S. Krishnamurthy, R. Goodhue, J. Hutchison, V. Scardaci, A. C. Ferrari, J. N. Coleman, "High-yield production of graphene by liquid-phase exfoliation of graphite", *Nat. Nanotech.*, vol. 3, p. 563-568, 2008.
- [68] M. Lotya, Y. Hernandez, P. J. King, R. J. Smith, V. Nicolosi, L. S. Karlsson, F. M. Blighe, S. De, Z. Wang, I. T. McGovern, G. S. Duesberg, J. N. Coleman, "Liquid Phase Production of Graphene by Exfoliation of Graphite in Surfactant/Water Solutions", *Am. Chem. Soc.*, vol. 131, p. 3611-3620, 2009.
- [69] X. An, T. Simmons, R. Shah, C. Wolfe, K. M. Lewis, M. Washington, S. K. Nayak, S. Talapatra, S. Kar, "Stable aqueous dispersions of noncovalently functionalized graphene from graphite and their multifunctional high-performance applications", *Nano Lett.*, vol. 10, p. 4295-4301, 2010.
- [70] M. S. Dresselhaus and G. Dresselhaus, "Intercalation compounds of graphite", *Adv. in Physics*, vol. 51, p. 1-186, 2002.
- [71] M. S. Dresselhaus., "Layered crystals and intercalated compounds", *Adv. in Solid State Phys.* Vol. 25, pp 21-37, 1985.
- [72] F. L. Vogel, "The Electrical Conductivity of Graphite Intercalated with Superacid Fluorides: Experiments with Antimony Pentafluoride", F. L. Vogel.
- [73] M. Winter, J. O. Besenhard, M. E. Spahr, P. Novák, "Insertion electrode materials for rechargeable lithium batteries", *Adv. Mater.*, vol. 10, p. 725-763, 1998.
- [74] E. Frackowiak, F. Béguin, "Carbon materials for the electrochemical storage of energy in capacitors", *Carbon*, vol. 39, p. 937-950, 2001.

References

- [75] W. Liu, H. Li, C. Xu, Y. Khatami, K. Banerjee, "Synthesis of high-quality monolayer and bilayer graphene on copper using chemical vapor deposition", *Carbon*, vol. 49, pp. 4122-4130, 2011.
- [76] G. Wang, B. Wang, J. Park, Y. Wang, B. Sun, J. Yao, "Highly efficient and large-scale synthesis of graphene by electrolytic exfoliation", *Carbon*, vol. 47, p. 3242-3246, 2009.
- [77] J. Wang, K. K. Manga, Q. Bao, K. P. Loh, "High-yield synthesis of few-layer graphene flakes through electrochemical expansion of graphite in propylene carbonate electrolyte.", *J. Am. Chem. Soc.*, vol. 133, p. 8888-8891, 2011.
- [78] C.-Y. Su, A.-Y. Lu, Y. Xu, F.-R. Chen, A. N. Khlobystov, L.-J. Li, "High-Quality Thin Graphene Films from Fast Electrochemical Exfoliation", *ACS nano*, vol. 5, p. 2332-2339, 2011.
- [79] M. Alanyahoğlu, J. J. Segura, J. Oró-Solè, N. Casañ. "The synthesis of graphene sheets with controlled thickness and order using surfactant-assisted electrochemical processes", *Carbon*, vol. 50, pp. 142-152, 2012.
- [80] A. K. G. S. V. M. E. W. H. P. B. M. I. K. a. K. S. N. F. Schedin, "Detection of individual gas molecules adsorbed on graphene", *Nat. Mater.*, vol. 6, p. 652-655, 2007.
- [81] E. Yoo, J. Kim, E. Hosono, H.-s. Zhou, T. Kudo, I. Honma, "Large reversible Li storage of graphene nanosheet families for use in rechargeable lithium ion batteries", *Nano Letter*, vol. 8, p. 2277-2282, 2008.
- [82] S. Stankovich, D. A. Dikin, G. H. B. Dommett, K. M. Kohlhaas, E. J. Zimney, E. A. Stach, R. D. Piner, S. T. Nguyen, R. S. Ruoff, "Graphene-based composite material", *Nature*, vol. 442, p. 282-286, 2006.
- [83] J. Longun, J. O. Iroh, "Nano-graphene/polyimide composites with extremely high rubbery plateau modulus extremely high rubbery plateau modulus", *Carbon*, vol. 50, p. 1823-32, 2012.
- [84] T. Ramanathan, A. A. Abdala, S. Stankovich, D. A. Dikin, M. Herrera-Alonso, R. D. Piner, D. H. Adamson, H. C. Schniepp, X. Chen, R. S. Ruoff, S. T. Nguyen, I. A. Aksay, R. K. Prud'Homme, L. C. Brinson, "Functionalized graphene sheets for polymer nanocomposites", *Nat Nanotechnol*, vol. 3, p. 327-331, 2008.

- [85] J. Liang, Y. Huang, L. Zhang, Y. Wang, Y. Ma, T. Guo, Y. Chen, "Molecular-Level Dispersion of Graphene into Poly (vinyl alcohol) and Effective Reinforcement of their Nanocomposites", *Adv. Funct. Mater.*, vol. 19, p. 2297-2302, 2009.
- [86] X. Zhao, Q. Zhang, D. Chen, "Enhanced Mechanical Properties of Graphene-Based Poly (vinyl alcohol) Composites", *Macromolecules*, vol. 43, p. 2357-2363, 2010.
- [87] L. Gong, R. J. Young, I. A. Kinloch, I. Riaz, R. Jalil, K. S. Novoselov., "Optimizing the Reinforcement of Polymer-Based Nanocomposites by Graphene", *ASC Nano*, vol. 6, pp. 2086-2095, 2012.
- [88] M. Noel, R. Santhanam, M. F. Flora, "Comparison of fluoride intercalation/de-intercalation processes on graphite electrodes in aqueous and aqueous methanolic HF media", *Power Sources*, vol. 56, p. 125-131, 1995.
- [89] D. W. Skaf, J. K Edwards, "Electrochemical graphite intercalation with nitric acid solutions", *Synthetic Metals*, vol. 46, p. 137-145, 1992.
- [90] D. Alliaata, R. Kötz, O. Haas, H. Siegenthaler, "In situ AFM study of interlayer spacing during anion intercalation into HOPG in aqueous electrolyte", *Langmuir*, vol. 15, p. 8483-8489, 1999.
- [91] M. D. Levi, D. Aurbach, "The mechanism of lithium intercalation in graphite film electrodes in aprotic media. Part 1. High resolution slow scan rate cyclic voltammetric studies and modeling", *Electroanal Chem.*, vol. 421, p. 79-88, 1997.
- [92] H.-P. Zhao, X.-Q. Feng, H. Gao, "Ultrasonic technique for extracting nanofibers from nature materials", *Apply Physic Letter*, vol. 90, pp. 073112-2, 2007.
- [93] S. H. Aboutalebi, M. M. Gudarzi, Q. B. Zheng, J.-K. Kim, "Spontaneous Formation of Liquid Crystals in Ultralarge Graphene Oxide Dispersions", *Adv. Funct. Mater.*, vol. 21, p. 2978-2988, 2011.
- [94] A. C. Ferrari, J. Robertson, "Interpretation of raman spectra of disordered and amorphous carbon", *Physical Review B*, vol. 61, p. 14095-14107, 2000.
- [95] O. Akhavan, "The effect of heat treatment on formation of graphene thin films from graphene oxide nanosheets", *Carbon*, vol. 48, p. 509-519, 2010.

References

- [96] Z. Ni, Y. Wang, T. Yu, Z. Shen, "Raman Spectroscopy and Imaging of Graphene", *Nano Research*, vol. 1, pp. 273-291, 2008.
- [97] K. N. Kudin, B. Ozbas, H. C. Schniepp, R. K. Prud'homme, I. A. Aksay, R. Car, "Raman Spectra of Graphite Oxide and Functionalized Graphene Sheets", *Nano Letter*, vol. 8, pp. 36-41, 2008.
- [98] Y. Wang, S. Serrano, J. J Santiago-Avilés, "Raman characterization of carbon nanofibers prepared using electrospinning", *Synthetic Metals*, vol. 138, p. 423-427, 2003.
- [99] B. Zhang, T. Wang, S. Liu, S. Zhang, J. Qiu, Z. Chen, H. Cheng, "Structure and morphology of microporous carbon membrane materials derived from poly (phthalazinone ether sulfone ketone)", *Microporous and Mesoporous Materials*, vol. 96, p. 79-83, 2006.
- [100] L. G. Cançado, A. Jorio, E. H. Martins Ferreira, F. Stavale, C. A. Achete, R. B. Capaz, M. V. O. Moutinho, A. Lombardo, T. S. Kulmala, A. C. Ferrari, "Quantifying Defects in Graphene via Raman Spectroscopy at Different Excitation Energies", *Nano Lett.*, vol. 11, pp. 3190-3196, 2011.
- [101] A. Dato, Z. Lee, K.-J. Jeon, R. Erni, V. Radmilovic, T. J. Richardson, M. Frenklach, "Clean and highly ordered graphene synthesized in the gas phase", *Chem. Comm.*, vol. 40, pp. 6095-6097, 2009.
- [102] E.-Y. Choi, T. H. Han, J. Hong, J. E. Kim, S. H. Lee, H. W. Kim, S. O. Kim, "polymers, Noncovalent functionalization of graphene with end-functional", *J. Mater. Chem.*, vol. 20, p. 1907-1912, 2010.
- [103] P. Ramesh, S. Bhagyalakshmi, S. Sampath, "Preparation and physicochemical and electrochemical characterization of exfoliated graphite oxide", *J. Coll. Int. Sci.*, vol. 274, p. 95-102, 2004.
- [104] S. D. Moon, Y. S. Kang, D. J. Lee, "Monte Carlo Simulation of the Molecular Properties of Poly (vinyl chloride) and Poly (vinyl alcohol) Melts", *Macromolecular research*, vol. 15, pp. 491-497, 2007.
- [105] X. Yang, L. Li, S. Shang, X.-m. Tao, "Synthesis and characterization of layer-aligned poly (vinyl alcohol)/graphene nanocomposites", *Polymer*, vol. 51, pp. 3431-3435, 2010.

- [106] J. R. Potts, D. R. Dreyer, C. W. Bielawski, R. S. Ruoff, "Graphene-Based Polymer Nanocomposites", *Polymer*, vol. 52, pp. 5-25, 2011.
- [107] S. Rana, J. W. Cho, L. P. Tan, "Graphene-crosslinked polyurethane block copolymer nanocomposites with enhanced mechanical, electrical, and shape memory properties", *RSC Advances*, vol. 3, p. 13796-13803, 2013.
- [108] P. Song, Z. Cao, Y. Cai, L. Zhao, Z. Fang, S. Fu, "Fabrication of exfoliated graphene-based polypropylene nanocomposites with enhanced mechanical and thermal properties", *Polymer*, vol. 52, pp. 4001-4010, 2011.
- [109] J. Su, Q. Wang, R. Su, K. Wang, Qin Zhang, Q. Fu, "Enhanced compatibilization orientation of poly vinyl alcohol/gelatin composite fibers using carbon nanotubes", *Applied polymer science*, vol. 107, pp. 4070-4075, 2008.
- [110] S. K. Mallapragada, N. A. Peppas, "Dissolution Mechanism of Semicrystalline Poly (vinyl alcohol) in Water", *Polymer Science: Part B*, vol. 34, pp. 1339-1346, 1996.
- [111] Y. Xu, W. Hong, H. Bai, C. Li, G. Shi, "Strong and ductile poly (vinyl alcohol)/graphene oxide composite films with a layered structure", *Carbon*, vol. 47, p. 3538-3543, 2009.
- [112] J. Xu, Y. Hu, L. Song, Q. Wang, W. Fan, G. Liao, Z. Chen, "Thermal analysis of poly (vinyl alcohol)/graphite oxide intercalated composites", *Polym. Degrad. Stab.*, vol. 73, p. 29-31, 2001.

Appendix

Calculation of Enthalpy of Mixing

Consider an isolated volume of solvent, V_{sol} , and an isolated mass of graphite, M_G . The graphite can be considered as arranged in flakes of thickness T_1 and area, A_1 . The number of such flakes is $N_1 = \frac{M_G}{\rho_G T_1 A_1}$, where ρ_G is the graphite density.

The enthalpy of mixing of solvent and graphite can be found by calculating the energy required to separate all molecules (solvent/graphene sheet) to infinity minus the energy to bring them back together in the form of solvent-graphite dispersion, but with flakes of different thickness. This can be divided into five energetic components.

1. The energy required to separate all graphene sheets to infinity is given by the energy required to create the surfaces associated with the individual graphene sheets and so is related to the effective graphite surface energy, E_{sur}^G , which can be thought of as the inter-sheet binding energy per unit area of surface.

$$E_1^{NT} = N_1 \left[\left(\frac{T_1 A_1}{tA} \right) 2A - 2A_1 \right] E_{sur}^G \quad \text{Eq. 1}$$

where the term in the round brackets represents the number of graphene sheets per flake and the second term in the square brackets represents a correction for the outer surface of the flake. Here, t and A are the thickness and area of individual graphene sheets.

2. The energy required to remove all the solvent molecules to infinity is given by

$$E_1^{Sol} = V_{Sol} E_{Coh}^{Sol} - A_1^{Sol} E_{sur}^{Sol} \quad \text{Eq. 2}$$

Where E_{Coh}^{Sol} is the solvent cohesive energy, E_{Sur}^{Sol} is the solvent surface energy and A_1^{Sol} is the external surface area of the solvent.

3. The energy retrieved by bringing the graphene sheets back from infinity to form N_2 flakes of thickness, T_2 , and length, L_2 , is similar to E_1^{NT} and is given by

$$E_2^G = N_2 \left[\left(\frac{T_2 A_2}{tA} \right) 2A - 2A_2 \right] E_{Sur}^G \quad \text{Eq. 3}$$

Where $N_2 = \frac{M_G}{\rho_G T_2 A_2}$.

4. We can also calculate the energy released by bringing the solvent molecules back from infinity to form liquid but leaving voids to accommodate the reconstituted flakes:

$$E_2^{Sol} = V_{Sol} E_{Coh}^{Sol} - A_2^{Sol} E_{Sur}^{Sol} - A_{inter}^{G-sol} E_{Sur}^{Sol} \quad \text{Eq. 4}$$

Here A_2^{Sol} is the new solvent (outer) surface area, while A_{inter}^{G-sol} is the surface area of the voids, which will accommodate the flakes.

5. Finally we must calculate the interfacial energy associated with placing the flakes in the voids:

$$E_2^{G-Sol} = 2A_{inter}^{G-sol} E_{inter}^{G-Sol} = 2N_2 2A_2 E_{inter}^{G-Sol} \quad \text{Eq. 5}$$

Where E_{inter}^{G-Sol} is the solvent-graphite binding energy per unit area. The factor of two comes from the fact that we are passivating two surfaces, that of the graphene and that of the solvent.

The enthalpy of mixing is given by

$$\Delta H_{mix} = E_1^G + E_1^{Sol} - (E_2^G + E_2^{Sol} + E_2^{G-Sol}) \quad \text{Eq. 6}$$

This can be calculated using the expressions outlined above. A number of approximations can be made. One is that the solvent external surface area is the same before and after mixing with the graphite ($A_2^{Sol} \approx A_1^{Sol}$), a reasonable approximation at low graphite content. In addition, we assume that the flakes that exist in the graphite powder are much larger than those in the dispersion ($T_1 \gg T_2$). Including these approximations, this works out to be

$$\Delta H_{mix} = 2 \frac{M_G}{T_2 \rho_G} [E_{Sur}^G + E_{Sur}^{Sol} - 2E_{inter}^{G-Sol}] \quad \text{Eq. 7}$$

Finally, we note that the volume fraction of graphite, ϕ , is given by $\phi = \frac{M_G}{V_{mix} \rho_G}$, where V_{mix} is the volume of the mixture. Then:

$$\frac{\Delta H_{mix}}{V_{mix}} = 2 \frac{\phi}{T_2} [E_{Sur}^G + E_{Sur}^{Sol} - 2E_{inter}^{G-Sol}] \quad \text{Eq. 8}$$

In general, for materials that interact predominately by dispersive interactions we can estimate E_{inter}^{G-Sol} from the geometric mean approximation:

$$E_{inter}^{G-Sol} \approx [E_{Sur}^G E_{Sur}^{Sol}]^{1/2}$$

Substituting this in above we get

$$\frac{\Delta H_{mix}}{V_{mix}} \approx \frac{2}{T_{flake}} (\delta_G - \delta_{sol})^2 \phi \quad \text{Eq. 9}$$

where $\delta_G = \sqrt{E_{Sur}^i}$ and where we write T_2 as T_{flake} for clarity.

The solvent surface energy, E_{Sur}^{Sol} , is related to the surface tension, γ^i , by:

$$\gamma = E_{Sur}^{Sol} - T S_{Sur}^{Sol}$$

Where S_{Sur}^{Sol} is the solvent surface entropy. The surface entropy is a generic liquid property that tends to have values in the range 0.07-0.14 mJ/m²K.

From equation 9, we expect a minimal energy cost of exfoliation for solvents whose surface energy matches that of graphene. We can quantify the amount of graphite flakes dispersed as a function of solvent surface energy (calculated from surface tension). According to literature values of the nanotube/graphite surface energy (that is 70–80 $\text{mJ}\cdot\text{m}^{-2}$), it predicts that good solvents are characterized by surface tensions in the region of 40–50 $\text{mJ}\cdot\text{m}^{-2}$.

On the other hand based on the published paper by Turro et al. surface tension of 0.1 M SDS solution is around 40 $\text{mJ}\cdot\text{m}^{-2}$ which it shows that this electrolyte can be a good candidate for exfoliation of the graphite to produce SWGSs.

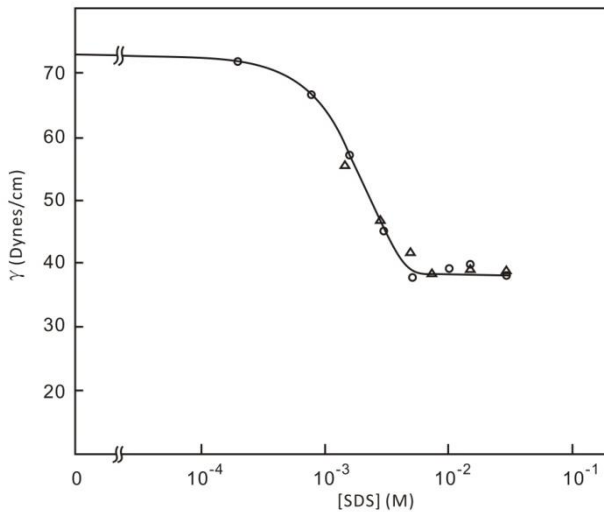


Fig. A1 Surface tension of SDS versus [SDS].

This book which is based on a master thesis is a contribution to the preparation/fabrication of graphene sheets and their properties regarding the specific applications through the following goals:

- Exploring a Novel Route for the Synthesis of a Stable Suspension Containing Graphene Sheets in Aqueous Solution.
- Characterization of the Produced Graphene Sheets.
- Developing the Graphene/Poly Vinyl Alcohol Nanocomposites.
- Evaluation of the Mechanical Properties of the Nanocomposites.



Mina Moradi

She was graduated in Material Science and Engineering at bachelor and master degree from Isfahan University of Technology (IUT) and Amirkabir University of Technology (AUT), Tehran, Iran respectively. She is a PhD candidate at Basel University, Basel, Switzerland at the moment.



Jamshid Aghazadeh Mohandesi

He was graduated from Sharif University of Technology, Tehran, Iran in B.S. in Metallurgical Engineering. For M.Sc. and PhD he moved to England and he was graduated at University of Manchester in Material Science and Engineering. At the moment he is a professor at AUT.



Davoud Fatmehsari Haghshenas

He was graduated from AUT, Tehran, Iran in B.S. in Materials Engineering-Extractive Metallurgy. For M.Sc. he moved to Sharif University of Technology, Tehran, Iran and for PhD he came back to AUT and was graduated at Materials Engineering-Extraction of Metals. At the moment he is an assistant professor at AUT.

To order additional copies of this book, please contact:
Science Publishing Group
book@sciencepublishinggroup.com
www.sciencepublishinggroup.com

ISBN 978-1-940366-41-8



9 781940 366418 >

Price: US \$80